

Effect of land use and groundwater flow path on submarine groundwater discharge nutrient flux



James M. Bishop^a, Craig R. Glenn^{a,*}, Daniel W. Amato^b, Henrietta Dulai^a

^a Department of Geology and Geophysics, University of Hawai'i at Mānoa, Honolulu, HI 96822, United States

^b Department of Botany, University of Hawai'i at Mānoa, Honolulu, HI 96822, United States

ARTICLE INFO

Article history:

Received 1 August 2015

Received in revised form 14 October 2015

Accepted 23 October 2015

Available online 14 November 2015

Keywords:

SGD

Nutrients

Isotopes

Tracers

Pollution

Coastal

ABSTRACT

Study region: Maui, Hawaii, United States.

Study focus: We investigated connections between land uses and submarine groundwater discharge (SGD) nutrient fluxes to coastal waters of Maui, Hawai'i. Nutrient contributions from agricultural lands, wastewater injection, and septic-cesspool systems were examined by combining a numerical groundwater model with $\delta^{18}\text{O}_{\text{H}_2\text{O}}$, $\delta^{15}\text{N}_{\text{NO}_3^-}$, and $\delta^{18}\text{O}_{\text{NO}_3^-}$ modeling to identify groundwater pathways, recharge elevations, and nitrate sources. Fresh and total SGD rates and nutrient fluxes were quantified using ^{222}Rn mass balance modeling.

New hydrological insights for the region: Low nitrate + nitrite (N + N) SGD fluxes (24 mols/d) were measured where groundwater flowed beneath primarily undeveloped land on transit to the coast. By contrast, of all land use types, sugarcane and pineapple fields contributed the largest amount of N to coastal waters via SGD (3800 mols/d). Despite their much smaller freshwater flux, these SGD sources provide substantially larger N fluxes than the State's largest rivers (avg. 700 mols/d). Septic systems, cesspools, and near coast wastewater injection wells also contribute N + N to groundwater and coastal waters, although in much smaller quantities. This study demonstrates that numerical groundwater modeling combined with geochemical modeling can be used to determine sources and flux of nutrients in SGD and provides a unique, original, and practical framework for studying the effect of land use and its impact on nutrient delivery to coastal waters.

© 2015 The Authors. Published by Elsevier B.V. This is an open access article under the CC BY-NC-ND license (<http://creativecommons.org/licenses/by-nc-nd/4.0/>).

1. Introduction

Fertilized agricultural lands, wastewater injection, and areas with high septic-cesspool system density each have potential for contributing excess nutrients to coastal waters of islands via submarine groundwater discharge (SGD). It has been hypothesized for the island of Maui that excess nutrient loading via SGD is a causal factor fueling the macroalgal blooms that have been smothering corals and fouling beaches since the late 1980's (e.g., Soicher and Peterson, 1997; Dollar and Andrews, 1997; Laws et al., 2004; Cesar and van Beukering, 2004; van Beukering and Cesar, 2004; Street et al., 2008; Dailer et al., 2010; Dailer et al., 2012). A first step in mitigating nutrient additions to coastal waters is to identify the source of nutrients. While methodologies for source tracking of nutrients to receiving waters from overland flow are well established (Borah and Bera, 2004), methods for determining nutrient sources in SGD are less well developed. The purpose of this study is to identify the sources of nutrients delivered to coastal waters via SGD.

* Corresponding author.

E-mail address: glenn@soest.hawaii.edu (C.R. Glenn).

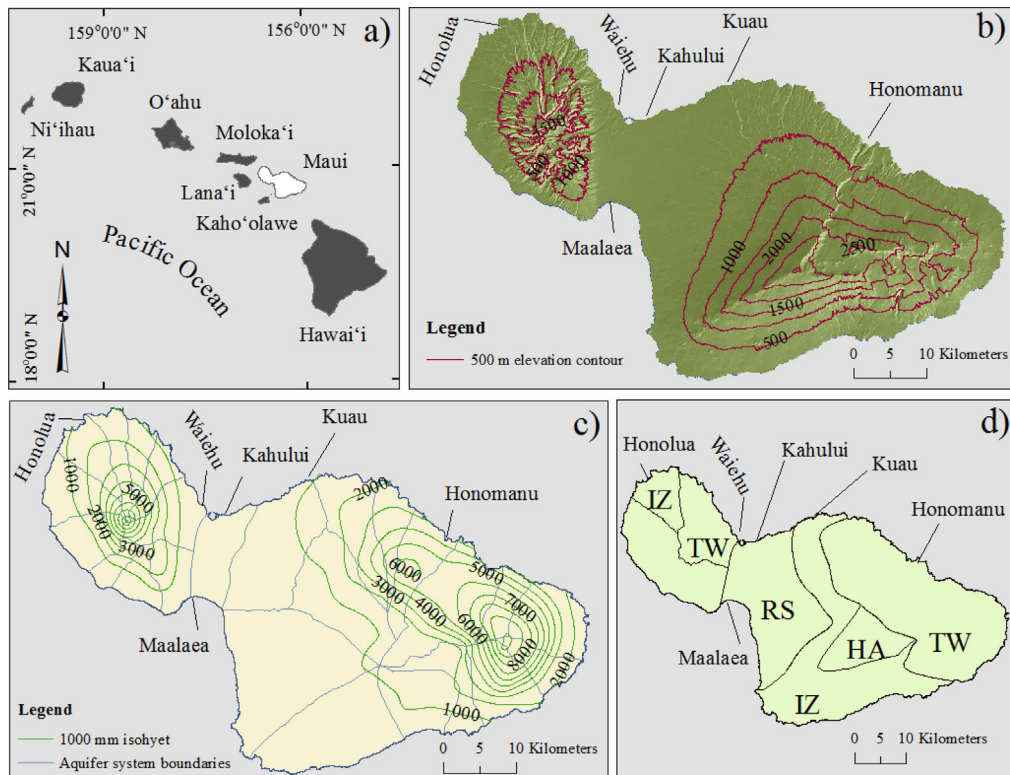


Fig. 1. (A) Hawaiian Islands with Maui shown in white. (B) Shaded relief map of Maui Island showing 500 m elevation contours. (C) Maui aquifer sectors in light blue and 1000 mm rainfall isohyets in green. (D) Local meteoric water line climate zones, adopted and modified from Scholl et al. (2002), were used in recharge elevation calculations. Coastal areas investigated during this study are indicated. Rainfall data from Giambelluca et al. (2013); DEM from NOAA (2007); aquifer sectors from State of Hawai'i (2008).

Relatively few studies have focused specifically on trying to identify the terrestrial source of nutrients in SGD. One such study on Long Island, New York found that high-density development was correlated with high nitrate discharge rates via SGD (Young et al., 2015). Another study on Kauai, Hawai'i found correlations between the amount of proximal agricultural land and nitrate plus nitrite (N + N) concentrations, which suggested fertilizers as the primary nitrogen source (Knee et al., 2008). On Hawai'i Island, similar correlations were found between N + N concentrations and proximity of golf courses, again implying fertilizer as the N source (Knee et al., 2010). Although such studies have strongly suggested a link between land use and SGD nutrient concentrations exists, they relied solely on correlations with proximal land use and did not consider the specific pathways taken by groundwater on transit to the coast.

In this paper we utilize a numerical groundwater model to identify the specific groundwater flow pathways to the coast, $\delta^{18}\text{O}$ of H_2O ($\delta^{18}\text{O}_{\text{H}_2\text{O}}$) to determine groundwater recharge elevations, $\delta^{15}\text{N}$ ($\delta^{15}\text{N}_{\text{NO}_3}$) and $\delta^{18}\text{O}$ ($\delta^{18}\text{O}_{\text{NO}_3}$) of dissolved nitrate to determine nitrate sources, and ^{222}Rn mass balance modeling to quantify fresh and total SGD rates. With these tools we (1) quantify the flux of nutrients to coastal waters via SGD in different areas of Maui, (2) identify specific land use practices that contribute nutrients to the coastal zone via SGD, and (3) calculate the flux of nutrients delivered to coastal zones from different land use practices. Our study demonstrates that numerical groundwater modeling combined with geochemical modeling is a robust method for determining the sources and flux of nutrients in SGD. The results presented here also illustrate how such work can provide site specific information of value to land use managers and planners regarding the magnitude of nutrients contributed to coastal waters from different land use practices.

2. Regional and hydrogeologic setting

The island of Maui (Fig. 1) is the second largest island in the Hawaiian Island chain. It is comprised of two separate basaltic shield volcanoes that overlap to form an isthmus between them (Stearns and Macdonald, 1942). The West Maui volcano has a maximum elevation of 1764 meters and Haleakala, the volcano comprising East Maui, has an elevation of 3055 m. Rainfall in Hawai'i is driven primarily by a combination of trade winds and orographic effect. Trade winds are persistent and blow from the northeast resulting in the north and eastern facing (windward) slopes generally receiving higher amounts of rainfall than south and west facing (leeward) slopes. Rainfall patterns in Hawai'i are extremely diverse and rainfall gradients can be exceptionally steep (see Giambelluca et al., 2011). On Maui, northeast facing, higher elevation areas can receive rainfall

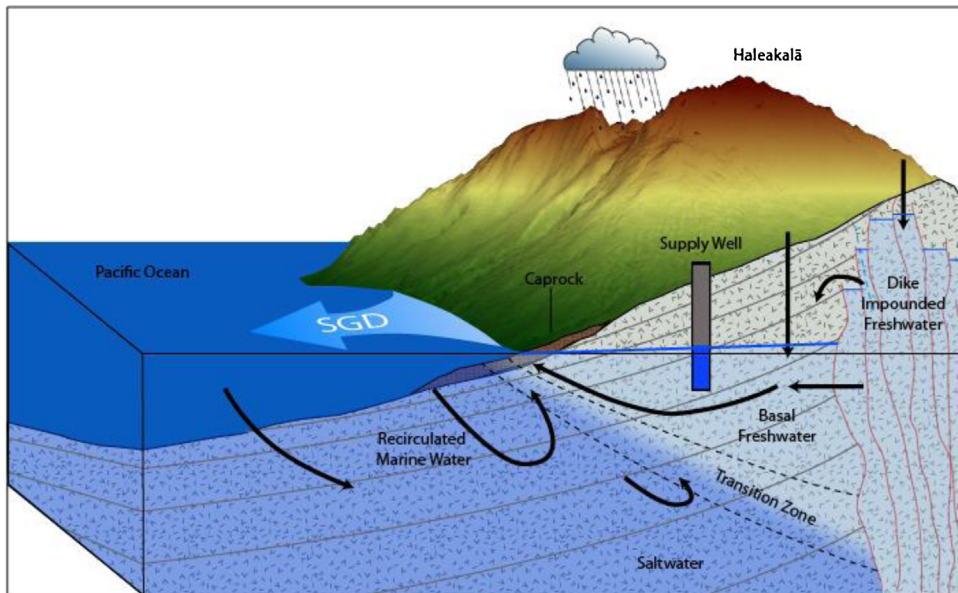


Fig. 2. Conceptual hydrogeologic model of groundwater and SGD flow on Maui. Not to scale.

Table 1

Field areas investigated in this study. The land uses assumed to contribute nutrients to groundwater and coastal water are listed.

Field area	Potential land use sources of nutrients
Kuau	Sugarcane, pineapple, moderate OSDS risk
Maalaea	Sugarcane, low-vol. wastewater injection
Kahului	Sugarcane, high-vol. wastewater injection, moderate OSDS risk
Honolua	Pineapple
Waiehu	High OSDS risk, sugarcane, macadamia orchards
Honomanu	Undeveloped land

upwards of 1000 cm per year, while the leeward Kihei region in southern Maui, one of the driest areas in the State, receives only 38 cm per year of rainfall on average (Giambelluca et al., 2013).

A conceptual hydrogeologic model for the island of Maui is shown in Fig. 2. The island was built primarily by interbedded basaltic lavas. Near vertical dikes of low permeability basalt radiate outward from the calderas of each volcano and cut through the bedded lavas. Along the coast and in the isthmus between the two volcanoes sedimentary deposits, locally termed ‘caprock’, impede the discharge of fresh groundwater at the coast (Engott and Vana, 2007). Fresh groundwater on Maui occurs primarily as either a basal freshwater system or high level, dike-impounded water. The basal freshwater system consists of a lens-shaped body of freshwater floating above more dense saline water that intrudes from the coast. Water levels in the basal system slope gently upward from the coast at a rate of about 0.3 m/km near Kahului (Burnham et al., 1977), though gradients can be much steeper in areas with substantial caprock. Unlike the basal system, dike impounded water can have hydraulic head thousands of feet above sea level due to the low permeability of dike rock (Engott and Vana, 2007), although the lateral extent of the dike impounded water is relatively small.

3. Methods

3.1. Land use and study sites

At low and moderate elevations forests dominate the landscape of wetter regions of Maui, while grasses, shrubs, and development cover drier areas. High elevations are dry and comprised of shrubs and grasslands. Central Maui is currently covered by approximately 160 km² of commercial sugarcane and had 45 km² of pineapple produced in the 1980’s, although pineapple cultivation has since been reduced to only 7 km² in 2015. In west Maui, pineapple and sugarcane were produced for most of the 20th century but sugarcane production ceased in 1999 and pineapple has not been cultivated since 2006.

To evaluate the effects of land use on nutrient concentrations to groundwater and coastal waters we chose coastal field areas that occurred downslope of specific dominant types of land use (Fig. 3; Table 1). Land use categories were based on a 2005 NOAA land cover map (NOAA, 2012) for Maui that delineated 25 land use types. We used these data to reclassify land use into three groups: agricultural land, developed land, and undeveloped land. An agricultural land use map from the State of Hawai’i Office of Planning, drafted between 1978 and 1980, was then used to subdivide the different types of agriculture.

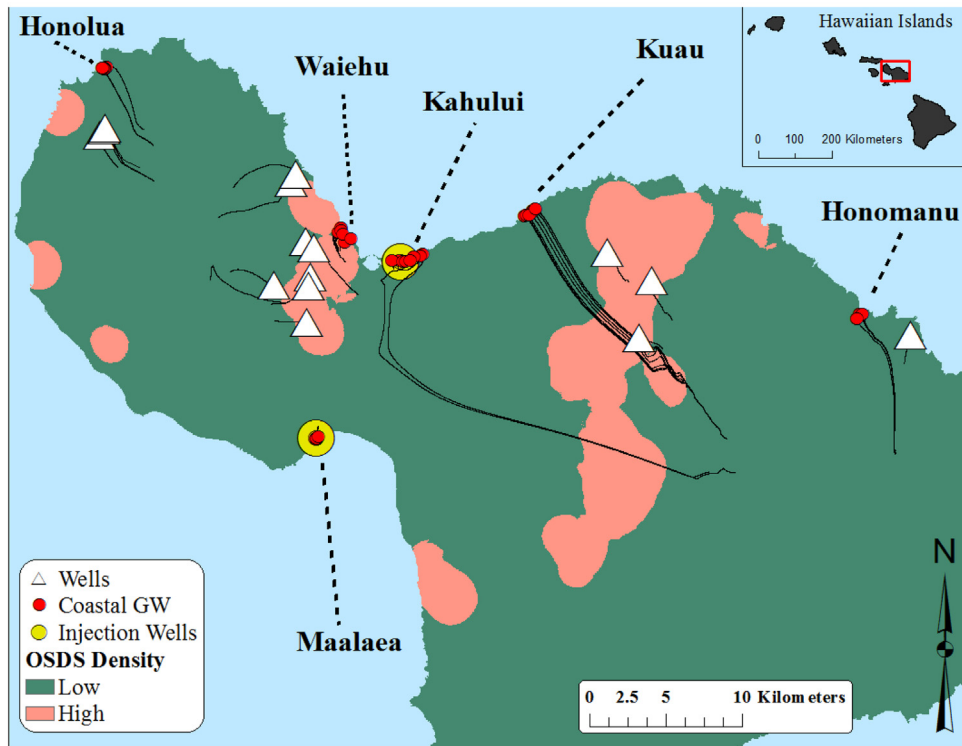
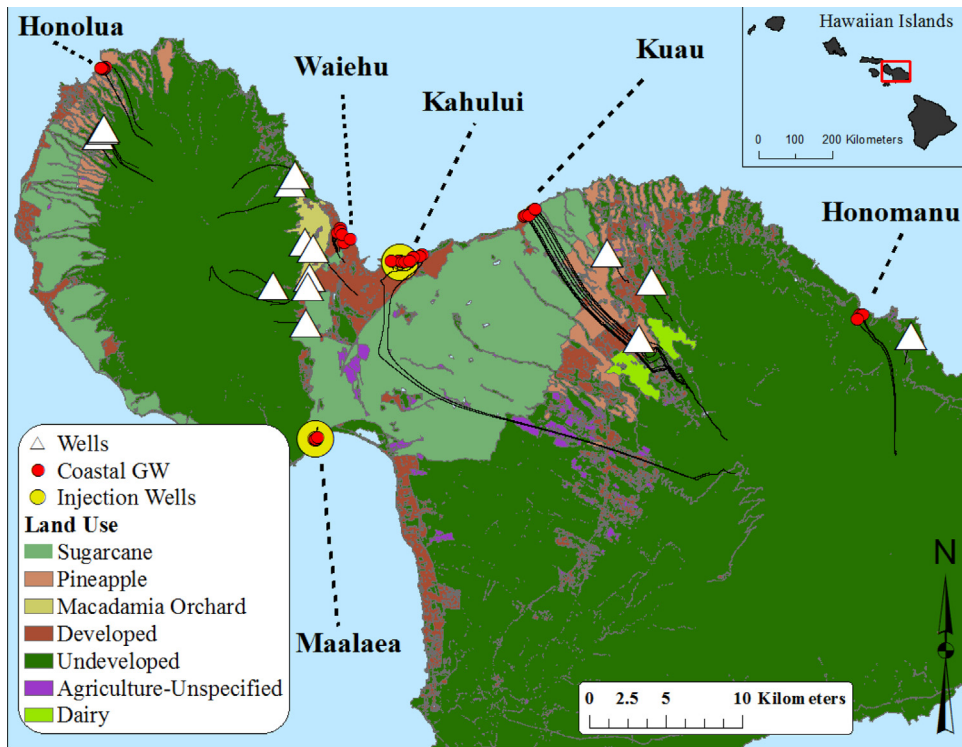


Fig. 3. Map of field sites. Land use (top) and OSDS density (bottom) are shown. Black lines indicate MODPATH derived groundwater flow paths (discussed below). Red circles indicate coastal groundwater sampling locations, white triangles are fresh groundwater supply well samples, and yellow dots show wastewater injection well locations utilized in this study.

Although more recent land cover maps exist (e.g., [Johnson et al., 2014](#) and references therein), we used the State of Hawai'i Office of Planning land use data because groundwater flow in Hawaiian aquifers occurs on multi-decadal scales ([Kelly and Glenn, 2015](#)) and hence chemical legacy effects of previous agricultural practices may still be present in the aquifers. The agricultural land use map was used to subdivide NOAA land cover agricultural polygons into five agricultural land use sub-categories: sugarcane; pineapple; macadamia orchards; agriculture unspecified; and commercial dairies. Only areas that were indicated as agricultural lands in the 2005 NOAA map were merged with the specific types of agriculture indicated in the 1978–1980 land use map. Unspecified agriculture are areas not specified by the State of Hawai'i agricultural land use map but are delineated as agricultural lands in the 2005 NOAA land cover map, i.e., areas that have become agricultural since the 1978–1980 land use map was drafted.

We also consider and overlay cesspools and septic tanks, collectively called on-site disposal systems (OSDS). OSDS risk to groundwater and coastal waters for different areas on Maui was estimated and ranked by [Whittier and El-Kadi \(2014\)](#) and is utilized in this study to identify areas to investigate for OSDS contamination. Areas are designated as either high or low OSDS density. High OSDS density are regions where OSDS exceeded 40 units/m², which is the density at which sufficiently maintained, properly working OSDS begin contaminating groundwater quality as determined by the USEPA ([Yates, 1985](#)). It is important to note that just a few malfunctioning OSDS can also have a contaminating effect on groundwater quality ([Robertson et al., 1991](#)). Wastewater injection wells were identified from the State of Hawai'i's Commission on Water Resources Management well index database and also integrated in our analysis. The County of Maui Wastewater Reclamation Division provided injectate volume and total nitrogen and phosphorus concentrations for the Kahului Wastewater Reclamation Facility.

3.2. Water sampling and analysis

Fieldwork was conducted during July 2012, July 2013, and March/April 2014. Water samples were collected from public water supply wells, coastal springs, beachface piezometers, and coastal surface waters. All samples were analyzed for the dissolved inorganic nutrients: silica (Si); nitrate and nitrite (N+N); ammonium (NH₄⁺); and phosphate (PO₄³⁻). For this study we used a Seal Analytical AA3 Nutrient Autoanalyzer at the University of Hawai'i SOEST Laboratory for Analytical Biogeochemistry (S-Lab). Over the course of the three sampling periods 30 nutrient samples were collected in duplicate and the uncertainty associated with duplicate analysis was calculated using relative percent difference (RPD; the absolute value of the difference as a percentage of the mean of the two samples). Average RPD was 4% for Si, 15% for N+N, 14% for PO₄³⁻, and 62% for NH₄⁺. Stable isotope analysis was conducted at the University of Hawai'i SOEST Biogeochemical Stable Isotope Laboratory. The δ¹⁸O_{H2O} in water was analyzed using a Picarro Cavity Ringdown Mass Spectrometer. Oxygen isotopic compositions of water were normalized to internal lab reference waters and are expressed in δ-notation in per mil (‰) relative to VSMOW. Samples with adequate nitrate concentration (≥ 1 μM) were analyzed for the nitrogen and oxygen isotopic composition of dissolved nitrate using the denitrifier method ([Sigman et al., 2001](#); [Casciotti et al., 2002](#); [McIlvin and Casciotti, 2011](#)). In samples that had a nitrite concentration greater than 1% of the nitrate concentration, nitrite was removed using sulfamic acid during sample preparation ([Granger et al., 2006](#)) prior to N and O isotopic analysis. Samples were analyzed on a Thermo-Finnigan MAT 252 mass spectrometer interfaced to a Thermo Finnigan Gasbench II with the Thermo Scientific Denitrification Kit. Analyses of N and O isotopic compositions of dissolved nitrate were normalized with nitrate-N and nitrate-O reference materials USGS-32, USGS-34, and USGS-35 relative to AIR and expressed in δ-notation in per mil (‰) relative to AIR and VSMOW, respectively. The error associated with duplicate analysis (*n* = 18) of stable isotopes, using the standard error of the estimate, was 0.05 ‰ for δ¹⁸O_{H2O}, 0.48 ‰ for δ¹⁸O_{NO3}, and 0.73 ‰ for δ¹⁵N_{NO3}. In situ temperature, salinity, conductivity, pH, and dissolved oxygen concentration were collected with multiparameter sondes (YSI 6600 V2-4, YSI EXO2) at the time of sample collection.

3.3. Coastal groundwater endmembers and salinity unmixing

In order to compare nutrient concentrations among field areas and assign a nutrient value to use in SGD nutrient flux calculations (described below) we determined coastal groundwater endmember nutrient concentrations representative of an entire field area. To do this, we normalize brackish coastal groundwater concentrations to the fresh groundwater concentration by fitting a linear regression to nutrient concentration versus salinity. Then, using the regression equation, we calculate the nutrient concentration that was equal to fresh groundwater salinity. The fresh groundwater salinity used to calculate nutrient endmember was the salinity of the most proximal public supply well sampled.

In order to compare the nutrient concentrations and δ¹⁸O_{H2O} values among individual samples that were collected with varying amounts of seawater dilution, samples were all 'unmixed' (normalized) to the fresh groundwater endmember as ([Hunt and Rosa, 2009](#)):

$$C_{fr} = C_{mix} + (C_{mix} + C_o) \times (S_{mix} + S_{fr}) / (S_o - S_{mix}) \quad (1)$$

where C_{fr} is the expected concentration or δ value of the fresh groundwater sample prior to seawater dilution, C_{mix} is the concentration or δ value of the sample to be unmixed, C_o is the concentration or δ value of the oceanic endmember, S_{mix} is the salinity of the sample to be unmixed, S_{fr} is the salinity of the fresh groundwater endmember, and S_o is the salinity of the oceanic endmember. Eq. (1) removes nutrient concentration dilution and ¹⁸O enrichment that results from freshwater

mixing with seawater so that all results can be directly compared on a freshwater-only basis. Salinity unmixed $\delta^{18}\text{O}$ values are used in calculating groundwater recharge elevations (Section 3.4). Unmixed concentrations or δ values for samples from a particular field area were calculated using endmembers specific to that area. The marine salinity and concentration used in Eq. (1) were from the highest salinity coastal water sample from a particular area. The fresh groundwater salinity was chosen from the well most proximal to each field area. Salinities in wells ranged from 0.05 to 0.40.

3.4. Groundwater flowpaths

Groundwater flowpaths were determined using a combination of MODFLOW modeled groundwater heads (Whittier et al., 2010), MODPATH, the oxygen isotopic composition of water, groundwater recharge data, and local meteoric water lines for different climate zones (Scholl, 2002). MODFLOW (Harbaugh, 2005) is a three-dimensional finite difference groundwater model used to calculate steady state and transient groundwater flow. MODPATH (Pollock, 2012) is a model that computes three dimensional groundwater flowpaths, called particle paths, using the output from MODFLOW modeled groundwater heads. Using MODPATH, we tracked simulated particles from the sampling location to the modeled particle origin. For wells, particle paths were created at the bottom of the screened interval of the well. Coastal groundwater particle paths were created at the bottom of the four-layer model (Whittier et al., 2010) in order to generate particle paths that best reflected actual flowpaths in the basal lens. The origin of each coastal groundwater path was subsequently modified after calculating the recharge elevation using the methods of Scholl et al. (1996) and described below.

Recharge elevations and particle path origins were determined using a groundwater recharge rate raster file (10 m \times 10 m resolution; Whittier and El-Kadi, 2014), the $\delta^{18}\text{O}_{\text{H}_2\text{O}}$ in coastal groundwater samples, and the local meteoric water lines of Scholl et al. (2002). Because aquifers on Maui are mostly unconfined (Gingerich, 2008), except for carbonate caprock that occurs near the coast (Stearns and Macdonald, 1942), the isotopic composition of fresh coastal groundwater can be assumed to represent the integration of isotopic compositions in precipitation that fell along the entire groundwater flowpath (Scholl et al., 1996). We assume there is no net isotopic fractionation between the precipitation and recharge. The isotopic composition of fresh coastal groundwater is the recharge-weighted average of the isotopic composition of precipitation from the recharge elevation to the coast. Recharge elevation is determined by finding the elevation at which measured groundwater isotopic composition matches the calculated, recharge-weighted, isotopic composition following the equation of Scholl et al. (1996):

$$\delta^{18}\text{O}_{\text{sample}} = \frac{\sum_{\text{elev}=1}^n (\delta^{18}\text{O})_n (R)_n}{\sum_{\text{elev}=1}^n (R)_n} \quad (2)$$

where $(\delta^{18}\text{O})_n$ is the isotopic value of precipitation calculated for raster cell n , $(R)_n$ is the recharge rate of raster cell n , and $\delta^{18}\text{O}_{\text{sample}}$ is the measured $\delta^{18}\text{O}$ value in the groundwater sample. A raster dataset of the isotopic composition of precipitation was created by multiplying the elevation in each cell of a 10 m vertical resolution digital elevation model (NOAA, 2007) by the $\delta^{18}\text{O}$ in precipitation vs. elevation regression equations for the different climate zones from Scholl et al. (2002). Particle paths are shown in Fig. 3. An important caveat is that MODPATH does not take in to account dispersion, which may be an important component in determining particle path trajectories if there is a high dissolved load. As such, the particle paths presented are idealized paths.

The elevation versus isotopic composition of precipitation relationships developed by Scholl et al. (2002) were defined for different climates zones on Maui and include the trade wind zone (TW), rain shadow zone (RS), and high altitude zone (HA) (Fig. 1). The TW encompassed samples from Honomanu and the RS encompassed samples from Kahului and Maalaea. To better characterize samples from Kuau, which were located in the transition between the TW and RS, we created a third climate zone called the intermediate zone (IZ). The IZ has a slope and intercept that is the mean of the slopes and intercepts from the TW and RS zones and was nearly parallel to the isotopic composition versus slope regressions of those two zones. Similar elevation versus precipitation relationships have not been developed for West Maui and as such there is no pre-defined climate zone to apply to the Waiehu and Honolua field areas. We assigned the elevation versus precipitation relationship that was most suitable for Waiehu and Honolua based on our knowledge of rainfall, trade winds, and measured groundwater isotopic compositions.

3.5. Statistical analysis

We conducted a multiple regression analysis to identify a linear relationship between the salinity unmixed nutrient concentration measured at all sampling locations (dependent variable) and the length of different land use types overlying all groundwater flow paths (independent variables). An F-test was used at the 95% confidence level to test for significance. Key assumptions of multiple linear regression relevant to this analysis include linearity between independent and dependent variables, normality of residuals, and homoscedasticity (Keith, 2006). All key assumptions were examined and are presented with the results.

3.6. Submarine groundwater discharge rates and nutrient fluxes

In order to quantify submarine groundwater discharge rates at each field area we used stationary radon time series to conduct a non-steady-state mass-balance model (Burnett and Dulaiova, 2003). We coupled the time series calculated rates with radon coastal surface water surveys (Dulaiova et al., 2010) to scale the stationary time series calculated fluxes by the mean fluxes measured along the coastline transected by the coastal survey, as detailed below. Radon in surface waters was measured using a radon-in-air monitor (RAD-Aqua, Durrige Inc., Billerica MA, USA) connected to an air-water exchanger that received water from a peristaltic pump (time series) or a bilge pump (surveys). Conductivity, temperature, and depth (CTD) were monitored at the pump hose inlet (time series and survey), as depth profiles along the surveys, and on the seafloor bottom (time series). Wind speed and air temperature were collected from either Kahului (WBAN 22516) or Kapalua (WBAN 22552) airport weather stations. For the mass-balance models we used an atmospheric radon activity of 30 dpm/m³ (Kelly, 2012), ²²⁶Ra supported ²²²Rn activity of 79 dpm/m³ (as measured by Street et al. (2008) at station MA3 on Maui), and an offshore ²²²Rn activity of 64 dpm/m³, which was derived from its parent ²²⁶Ra activity identified by Street et al. (2008). The residence times of the groundwater signature within coastal surface water were assumed to be 12.42 h, the length of a tidal cycle. Discrete coastal groundwater samples were analyzed within 12 h of collection using a RAD-H₂O system (Durrige), then time-corrected for decay.

3.6.1. Stationary time series measurements

All radon time series were conducted during March and April 2014 except for Kuau, which was conducted July 2013. Radon measurements were integrated over 30 min periods. The peristaltic pump hose inlet was attached to the bottom of a float in order to ensure that the pump inlet was as close as possible to the ocean water surface throughout the course of the deployment. A salinity depth profile was collected at the time series location in order to characterize the thickness of the mixed-salinity brackish SGD plume, which disperses from land and floats on top of marine water. In order to account for changes in the thickness of the brackish SGD plume over a tidal cycle, we subtracted the marine layer thickness measured during the depth profile from the total depth of the water column measured by the CTD. We then scaled the ²²²Rn inventories to the depth of the mixed-salinity SGD layer at the corresponding cycle.

3.6.2. Radon surface water surveys

Surface water surveys were conducted during July 2013 with the exception of Maalaea and Honolulu, which were conducted in March 2014 and August 2012, respectively. Radon surveys were conducted by motoring a boat parallel to shore at ≤5 km/hr while the bilge pump supplied surface water to the air-water exchanger. Radon measurements were integrated over 5 min periods. The SGD fluxes were calculated using the ²²²Rn box model of Dulaiova et al. (2010). The coastal boxes used were determined as the perpendicular distance from the shore to each radon data point, and the half distance from one data point to the other along the shore. The depth of the coastal box was the thickness of the mixed salinity layer determined by salinity depth profiles, which were taken periodically.

3.6.3. SGD flux scaling

While survey-calculated fluxes have been used as standalone measurements of discharge rates (Burnett and Dulaiova, 2003; Dulaiova et al., 2005; Dulaiova et al., 2010), these only represent a snapshot of SGD rates and not a tidal average. We therefore used the survey calculated fluxes in a relative sense to scale the time series calculated flux. The time series SGD flux was normalized to shoreline length (m³/m/d). The SGD determined during the survey, which only represents a snapshot estimate, was also normalized to the corresponding shoreline length. A scaling factor was calculated by dividing each survey segment flux by the time series flux at the time series location. The mean scaling factor from the entire survey was multiplied by the time series flux in order to receive a tidal average SGD along the survey line. The SGD fluxes that were scaled as described above will be referred to as scaled total (fresh + saline) or scaled fresh fluxes.

This methodology thus combines the spatial resolution of the survey fluxes with the temporal resolution of the time series flux. The primary reason for using scaled SGD rates is that, for the purpose of understanding the effect of land use on coastal nutrient concentrations via SGD, it is more beneficial to calculate fluxes for the entire length of coastline affected by a particular type of land use, not just a single spring. A tacit assumption in the scaling is that the ratio of fresh groundwater to recirculated seawater in SGD remains constant over the survey area and the endmembers represent the whole section of the coastline surveyed. The other assumption inherent in the SGD flux scaling is that the trends captured by the surveys and time series are representative of the field site and there is no temporal variability between fluxes measured days or years apart.

3.6.4. Calculating fresh SGD flux and nutrient flux

The methods described above were used to calculate the total (fresh + saline) SGD fluxes. We assume that the land derived nutrients in SGD are contained primarily in the fresh portion of SGD. Therefore, in order to obtain a meaningful nutrient flux, we calculated the freshwater fraction of total SGD in order to obtain a freshwater SGD flux. Furthermore, this approach allowed for direct comparison of the fresh SGD nutrient flux to the freshwater nutrient flux from rivers in Hawai'i. The fresh SGD nutrient flux is then simply the product of the fresh SGD rate and the groundwater endmember nutrient concentration.

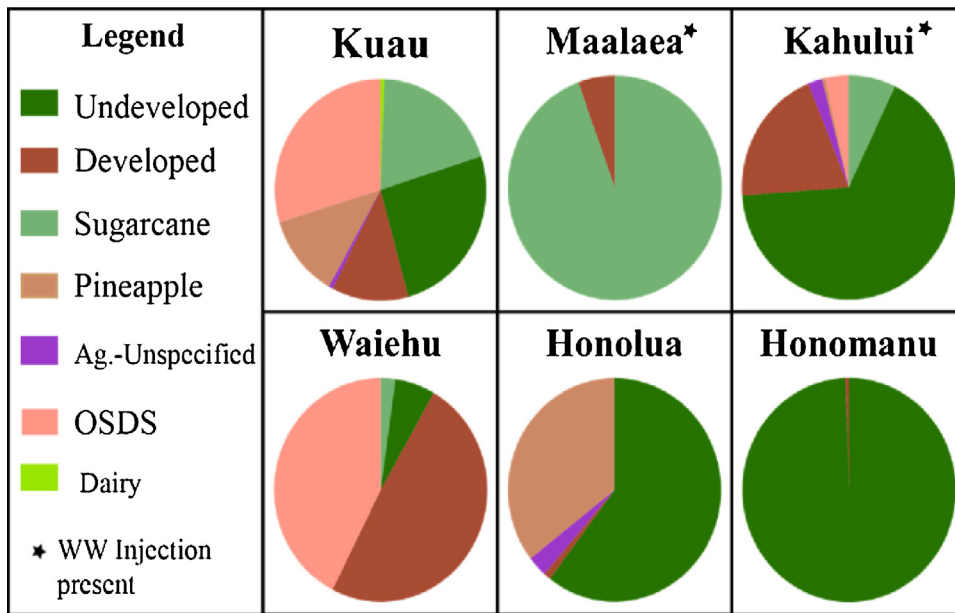


Fig. 4. Mean land use type transected by all coastal groundwater samples from each field area. Asterisks indicate areas that also contain wastewater injection wells.

To calculate the freshwater fraction of total SGD, a two endmember mixing analysis was employed using a system of two equations and two unknowns:

$$1 = f_o + f_{GW} \quad (4)$$

$$S_m = S_o f_o + S_{GW} f_{GW} \quad (5)$$

where f_o is the oceanic fraction of SGD, f_{GW} is the fresh groundwater fraction, S_{GW} is the salinity of groundwater measured in supply wells proximal to the field area, S_o is the salinity of the marine endmember, assumed to be 35.5 ppt, and S_m is the mean salinity measured in all samples collected from beachface seeps and piezometers at a particular field area. Beachface seep and piezometer samples were collected within three hours of low tide and thus are biased towards low tide coastal groundwater salinities, which is when most SGD occurs anyway.

4. Results

4.1. Land use

Land use categories transected by coastal groundwater samples on transit to the coast include developed land, undeveloped land, OSDS, sugarcane, pineapple, unspecified agriculture, and dairy farms. Fig. 4 illustrates the average land use types transected by coastal groundwater samples from a particular field area. Honomanu and Maalaea flowpaths transect principally (>90%) undeveloped land and sugarcane, respectively, while the other field areas are more mixed. The dominant type of land use transected by flowpaths at each of the field areas are: Kuau, 30% high density OSDS; Maalaea, 94% sugarcane; Kahului, 66% undeveloped; Waiehu, 49% developed; Honolulu, 60% undeveloped; and Honomanu, 99% undeveloped.

We examined how changes in recharge data can affect the calculated groundwater particle paths by re-running the numerical groundwater model with a different recharge coverage. We then used that coverage to calculate the recharge elevation (Eq. (2)). We utilized recharge data from Shade (1999) for east Maui and examined the types of land use transected by particle paths created for coastal groundwater samples from Kuau. The newly created particle paths had trajectories that were identical to the original particle paths, although the new paths were longer than the original paths. This new recharge coverage resulted in increasing the amount of undeveloped land transected by particle paths increasing by 14% while the other land use categories decreased by 6% or less. This analysis indicates that the types of land use transected by particle paths are sensitive to recharge data, although our analysis indicates that changes in recharge data primarily affect the length of the path, not path trajectory.

4.2. Salinity

Well samples had the lowest salinities and ranged from 0.05–0.40 (mean = 0.20, s.d. = 0.12), coastal groundwater sample had the largest range in salinities from 0.10–32.49 (mean = 7.24, s.d. = 8.00), and coastal surface water samples salinities

Table 2

Mean nutrient concentrations. Surface coastal water (CW) concentrations are shown in the top block, coastal groundwater (GW) samples are shown in the middle block, and well samples are shown at the bottom. Standard deviations, number of samples (n), and salinity ranges for each field area are shown.

Site	n	Salinity	PO ₄ ³⁻	Si	N + N	NH ₄ ⁺
Kuau—CW	12	28.01 - 35.71	0.31 ± 0.26	68 ± 53	23 ± 17	0.26 ± 0.34
Maalaea—CW	22	28.51 - 35.85	0.19 ± 0.29	28 ± 34	12 ± 18	0.77 ± 1.1
Kahului—CW	25	30.03 - 34.88	0.40 ± 0.81	78 ± 101	3.1 ± 4.3	0.33 ± 0.90
Honolulu—CW	16	30.26 - 35.02	0.09 ± 0.11	41 ± 29	1.4 ± 1.5	0.57 ± 1.0
Waiehu—CW	13	20.70 - 35.35	0.11 ± 0.23	34 ± 37	0.06 ± 0.07	0.55 ± 1.2
Honomanu—CW	11	32.52 - 34.74	0.24 ± 0.14	51 ± 30	0.18 ± 0.24	0.12 ± 0.26
Kuau—GW	10	0.88 - 20.24	4.3 ± 1.4	760 ± 139	377 ± 80	1.0 ± 1.4
Maalaea—GW	7	1.22 - 34.59	4.6 ± 2.8	387 ± 228	190 ± 98	0.25 ± 0.45
Kahului—GW	9	1.58 - 19.98	1.8 ± 0.65	497 ± 267	28 ± 28	14 ± 38
Honolulu—GW	9	0.40 - 19.50	1.5 ± 0.58	405 ± 95	25 ± 11	0.67 ± 0.76
Waiehu—GW	8	0.47 - 32.49	3.2 ± 2.7	354 ± 190	22 ± 40	1.5 ± 2.2
Honomanu—GW	7	0.1 - 13.5	3.1 ± 1.8	591 ± 260	6.4 ± 3.0	0.93 ± 1.3
Wells	18	0.05 - 0.42	3.0 ± 1.1	756 ± 100	28 ± 20	0.01 ± 0.02

Table 3

Coastal groundwater nutrient concentrations. Groundwater endmember concentrations are shown on the left with the standard error of the estimate indicated after the ± symbol. Mean, salinity-unmixed, coastal groundwater concentrations are shown on the right with the standard deviation shown after the ± symbol and the number of samples indicated by the n column.

Coastal groundwater endmember concentrations (μmol L ⁻¹)					Mean salinity unmixed coastal groundwater concentrations (μmol L ⁻¹)				
Site	PO ₄ ³⁻	Si	N + N	NH ₄ ⁺	n	PO ₄ ³⁻	Si	N + N	NH ₄ ⁺
Kuau	4.9 ± 0.8	884 ± 27	439 ± 22	0.9 ± 1.0	10	5.0 ± 1.3	889 ± 44	440 ± 35	1.7 ± 3.1
Maalaea	7.2 ± 0.6	611 ± 27	291 ± 17	0.4 ± 1.0	6	7.2 ± 1.4	609 ± 65	322 ± 70	0.3 ± ^{*5} 0.6
Kahului	2.4 ± 0.3	664 ± 132	55 ± 19	1.8 ± 1.9 ^a	9	2.4 ± 0.6	625 ± 250	36 ± 31	41 ± ^{*4} 62
Honolulu	1.8 ± 0.3	473 ± 24	29 ± 5.6	0.6 ± 1.0	9	1.8 ± 0.5	475 ± 30	29 ± 10	1.2 ± 1.0
Waiehu	2.5 ± 2.0	505 ± 59	37 ± 24	2.6 ± 1.4	8	6.7 ± 5.9	601 ± 225	33 ± ^{*7} 41	1.5 ± ^{*6} 2.6
Honomanu	3.4 ± 1.0	681 ± 153	7.9 ± 1.7	0.8 ± 0.8	7	3.3 ± 1.7	647 ± 236	7 ± 3	1.3 ± 1.8

Asterisk superscript numbers indicate the number of samples used in the mean calculation if nutrient concentrations in some samples were non-detectable.

^a Sample KWP-5 was omitted from the endmember calculation because of the anomalously high NH₄⁺ concentration of 118.3 μM.

ranged from 20.70–35.83 (mean = 32.86, s.d. = 3.16). Coastal water samples generally had lower salinities closer to shore and showed significant correlation between distance from shore and salinity at four of the six sites using Spearman's Rank correlation.

4.3. Groundwater and coastal water nutrient concentrations

Coastal groundwater, wells, and springs had highest N + N, Si, PO₄³⁻, and NH₄⁺ concentrations while nutrient concentrations in coastal surface water samples were much lower. Groundwater concentrations ranged from 0.02 μM to 460 μM for N + N, 0 to 115 μM for NH₄⁺, 0.28–8.53 for PO₄³⁻, and 54 to 899 for Si. Coastal water concentrations ranged from 0 to 59.6 μM for N + N, 0 to 4.8 for NH₄⁺, 0 to 4.1 μM for PO₄³⁻, and 0 to 518 μM for Si. NH₄⁺ was at or near detection for many samples. Mean coastal water nutrient concentrations are given in Table 2.

We examined correlations between distance from shore and nutrient concentration in coastal water samples using Spearman's rank correlation. Coastal water PO₄³⁻, Si, and N + N were significantly ($p < 0.05$) inversely correlated with distance from shore at four of the six field sites. Honomanu did not display a significant inverse relationship between distance from shore and any of the nutrient species in coastal water samples and NH₄⁺ was not significantly correlated with distance from shore at any of the field areas.

Linear regressions on N + N, PO₄³⁻, and Si versus salinity for all coastal surface water and coastal groundwater samples for each field area were all statistically significant ($\rho < 0.05$) and are shown in Fig. 5. Regressions on NH₄⁺ were not statistically significant. These regressions (Fig. 5) were used to determine groundwater endmember concentrations, shown in Table 3. The alternative method to determine the groundwater endmember concentration would be to salinity unmix all samples using Eq. (1) and then find the mean of all unmixed groundwater concentrations from a particular field area. Because regressions on nutrient concentration and O isotopic composition of water versus salinity were mostly significantly linear ($p < 0.05$), except for ammonium, the linear unmixing equation is appropriate. The results of either method are quite similar and are shown in Table 3, though the regression method generally resulted in more conservative estimates.

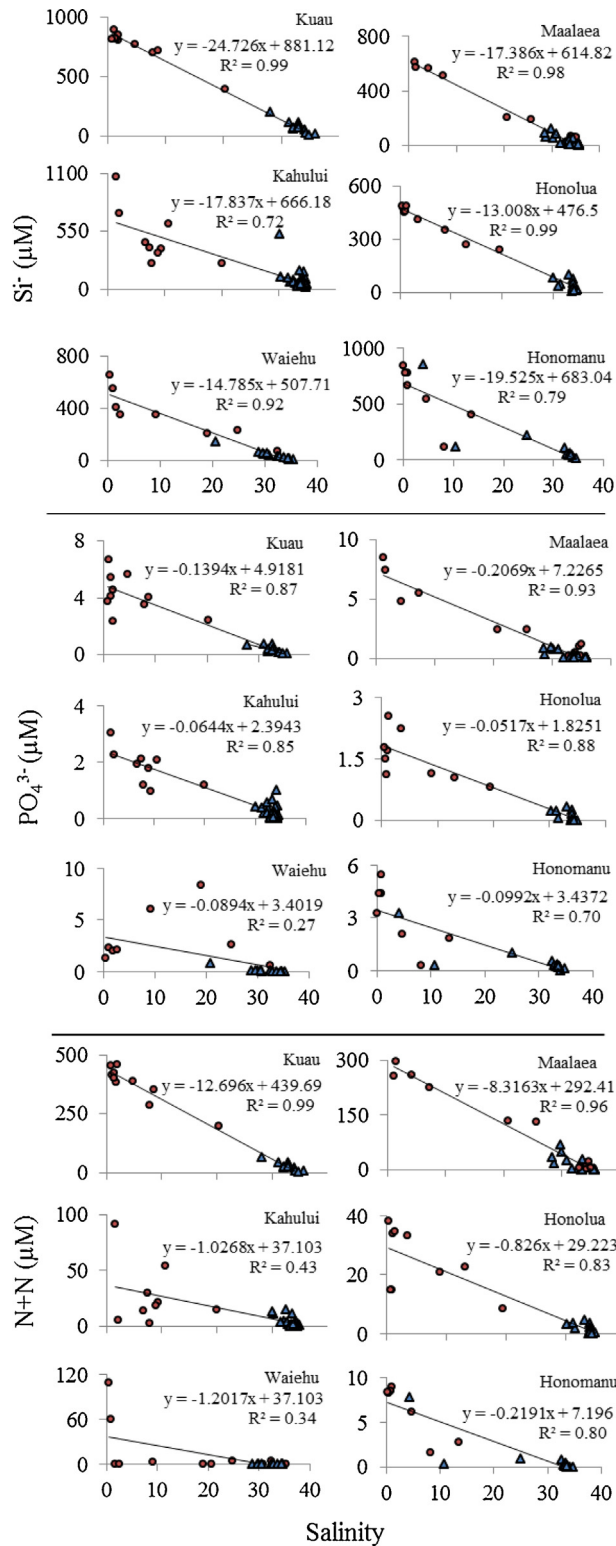


Fig. 5. N+H, PO₄³⁻, and Si vs. salinity used to derive coastal groundwater endmember values. Coastal groundwater samples are red circles and marine surface samples are blue triangles. Regression equations, best fit lines, and coefficients of determination are shown. All regression are significantly linear at $p < 0.01$ except for Waiehu PO₄³⁻, where $p = 0.02$.

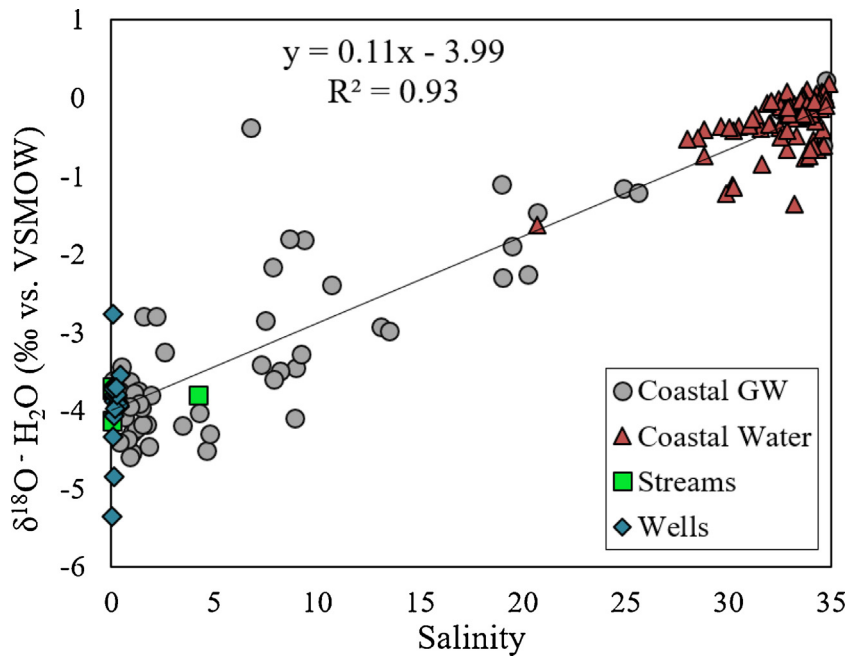


Fig. 6. $\delta^{18}\text{O}_{\text{H}_2\text{O}}$ versus salinity for all coastal groundwater (Coastal GW), coastal water, stream, and well samples collected during this study ($R^2 = 0.93$).

Table 4

Multiple regression equations and R^2 values for various nutrient species. Regression intercepts are indicated by the bold β symbol, independent land use type and dependent nutrient species are also bolded, and standardized coefficients are shown.

Regression Equation	R^2
$[\text{N} + \text{N}] = 68.2\beta + 1.32 \text{ Sugarcane} + 0.02 \text{ Pineapple} - 0.17 \text{ Undeveloped} - 0.95 \text{ Unspecified Ag.}$	0.81
$[\text{Si}] = 45.1\beta + 0.83\text{OSDS} - 0.26\text{Unspecified Ag.}$	0.29
$[\text{PO}_4^{3-}] = 3.67\beta + 0.4 \text{ Sugarcane} - 0.37\text{Unspecified Ag.}$	0.07

4.4. Isotopic composition of water

A strong linear correlation exists between the oxygen isotopic composition of water and salinity for all groundwater and coastal water samples (Fig. 6). The $\delta^{18}\text{O}$ of water in coastal water samples ranged from -3.8 to 0.2% and had a mean of -0.4% . The coastal groundwater samples had values ranging from -4.6% to 0.2% with a mean of -2.9% . Well samples had $\delta^{18}\text{O}_{\text{H}_2\text{O}}$ ranging from -5.4 to -2.8% with a mean of -4.0% .

4.5. N and O isotopic compositions of nitrate

The $\delta^{18}\text{O}_{\text{NO}_3}$ vs. $\delta^{15}\text{N}_{\text{NO}_3}$ values for combined coastal groundwater and coastal surface water samples from each field area along with a sample of treated wastewater effluent from Kahului wastewater treatment facility are shown in Fig. 7. The $\delta^{15}\text{N}_{\text{NO}_3}$ and $\delta^{18}\text{O}_{\text{NO}_3}$ values from all samples collected ranged from 0.3 to 44.1% for N and -3.8 to 22.6% for O. The highest mean $\delta^{15}\text{N}_{\text{NO}_3}$ values were from the Kahului field area (18.3%), and lowest mean values were from Honomanu (1.4%).

4.6. Multiple regression on land use and groundwater nutrient concentration

Regression was run on all land use variables initially, then re-run using only the statistically significant ($\rho < 0.05$) variables from the initial regression. Thus, we present results that reflect only analyses conducted on statistically significant independent variables. Regression equations with standardized coefficients are shown in Table 4. The regression on N + N had the highest R^2 value (0.81), was statistically significant ($F[4,61] = 66.693$, $\rho < 0.001$), and sugarcane and unspecified agriculture are the most significant independent variables ($\rho < 0.001$) followed by pineapple ($\rho = 0.006$) and undeveloped land ($\rho = 0.01$). A plot of the predicted versus measured N + N concentration is shown in Fig. 8. The regression on Si and PO_4^{3-} had R^2 values of 0.28 and 0.07; the regression on PO_4^{3-} was not significant. NH_4^+ was excluded in this analysis because of low and highly variable concentrations in groundwater samples. Regression residuals for all three nutrient species failed the Kolmogorov-Smirnov normality test, though q-q plots for N + N (not shown) indicate that the deviation from normality is not severe. Furthermore, regression analysis is quite robust against violations of normality and thus significance tests can still be performed even when this assumption is violated (Berry and Feldman, 1985). Adherence to assumptions of

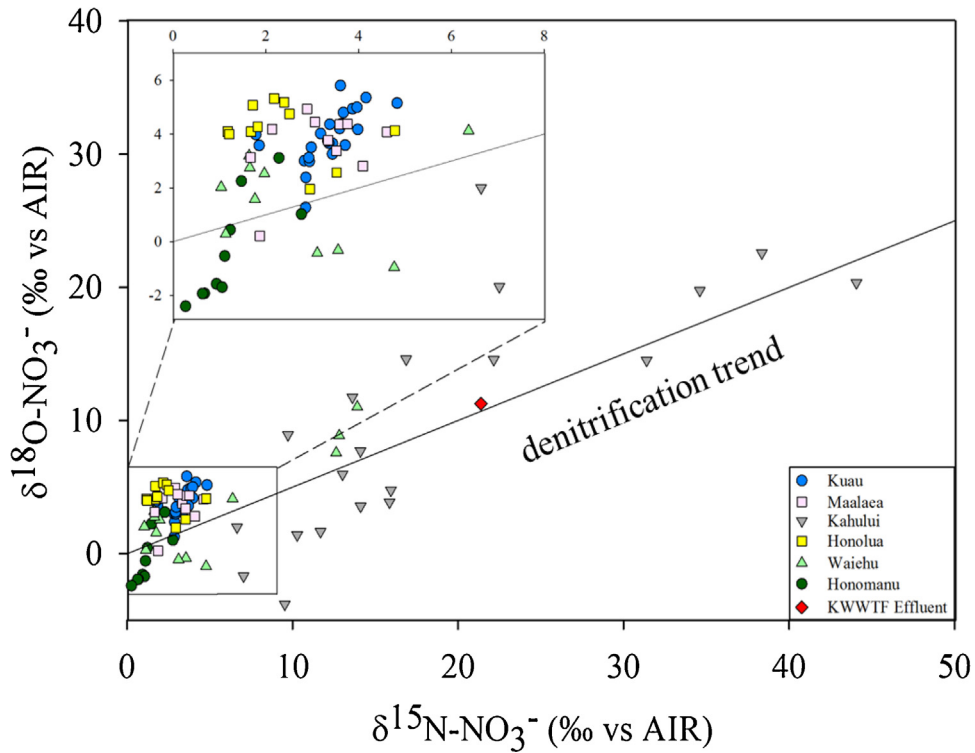


Fig. 7. $\delta^{18}\text{O}_{\text{NO}_3}$ vs. $\delta^{15}\text{N}_{\text{NO}_3}$ for all coastal water and coastal groundwater samples collected from each field area. The Kahului Wastewater Treatment Facility effluent sample composition is shown as a red diamond. Inset plot is a large-scale subset.

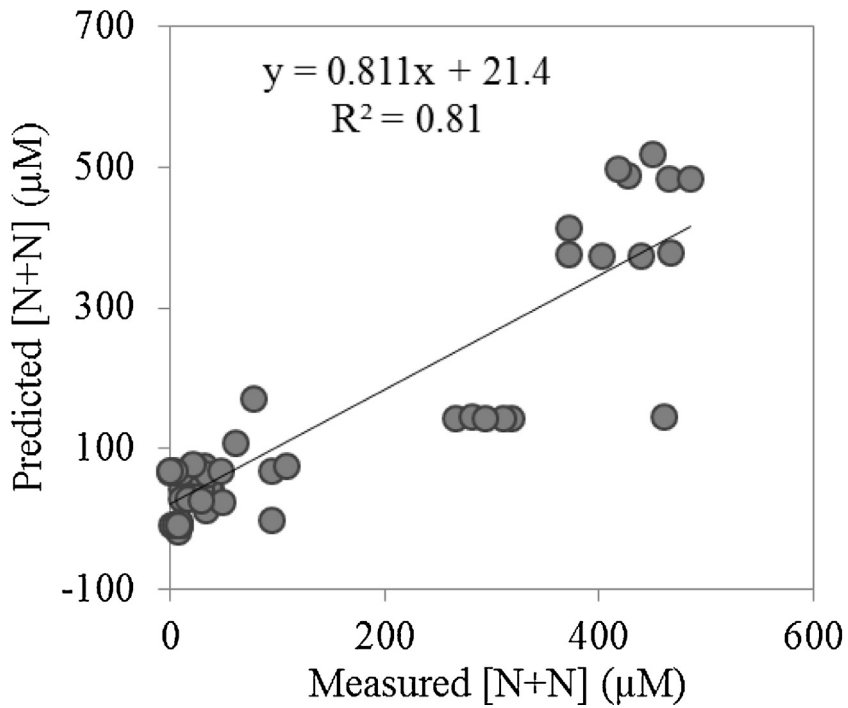


Fig. 8. N + N concentration predicted from multiple regression equation versus measured N + N concentration.

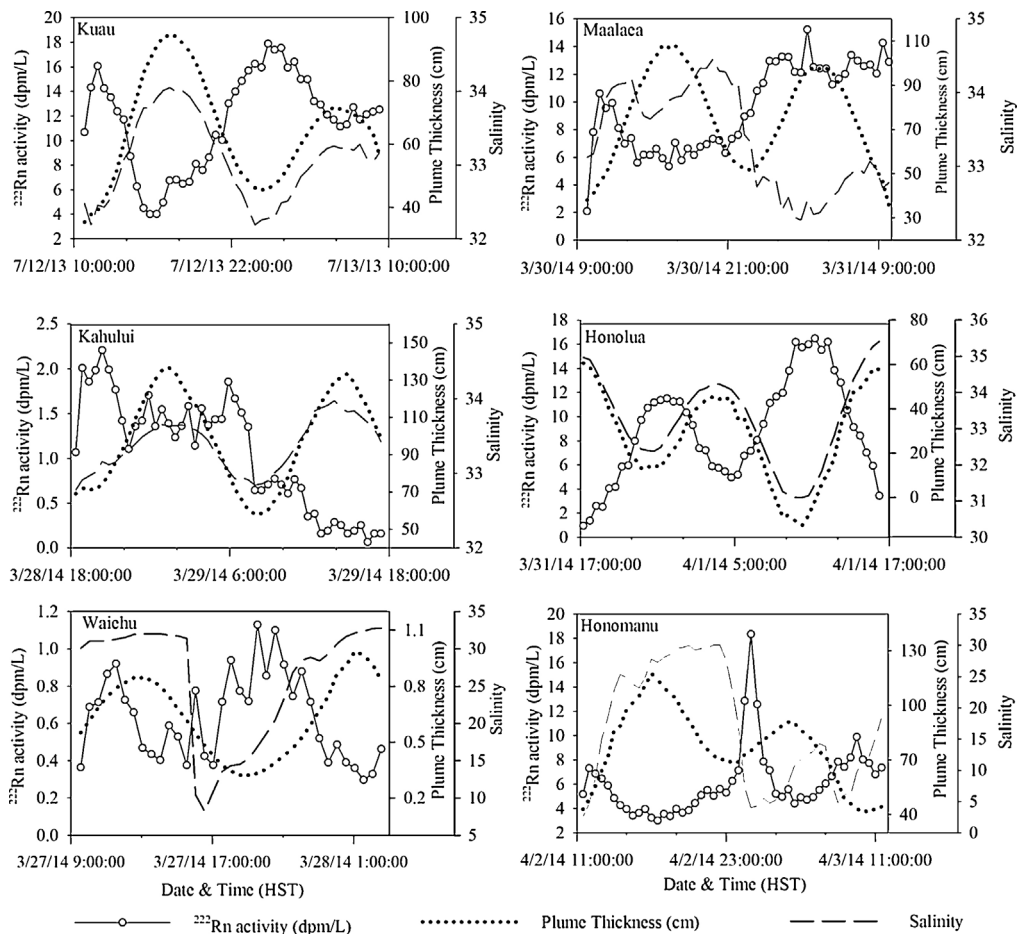


Fig. 9. ^{222}Rn activity, salinity, and mixed fresher layer SGD plume thickness measured at each coastal water stationary radon time series deployment. Individual ^{222}Rn measurements are shown as white circles, salinity as dashed lines, and plume thickness as black dots. Vertical scale varies from plot to plot in order to optimally display the full range of data.

homoscedasticity and linearity were investigated using plots of residuals versus predicted values (not shown) and residuals versus independent variables (not shown), respectively; these assumptions were not violated for any of the regressions.

4.7. Radon stationary time series

The ^{222}Rn activity measured in surface coastal waters during time series ranged from 0.06 to 18.3 dpm/L, salinity ranged from 2.59 to 34.82, and mixed salinity layer plume thickness varied from 0 to 139 cm (Fig. 9). The radon time-series measurements at sites that had lower activities (on average <2 dpm/L) resulted in a larger scatter (Kahului and Waichu) due to the lower sensitivity of the measurement and also a larger effect of waves and currents on the relatively small radon inventory. All the other records show a very well correlated relationship with tides and currents and salinity. SGD plume thickness and salinity were generally well correlated with each other and ^{222}Rn activity was inversely correlated. This is expected because salinity increases on a rising tide, the rising tide decreases the hydraulic gradient, groundwater discharge is reduced, and radon activity gets diluted by the larger incoming water mass.

SGD fluxes were normalized by the shore parallel length of the model polygon side in order to present discharge rates in terms of discharge volume per meter of shoreline per day. Important model parameters used in stationary time series SGD flux calculations are shown in Table 5. Mean SGD fluxes over an entire time series ranged from 1.1 to $6.9 \text{ m}^3/\text{m}/\text{d}$ for total SGD and 0.7 to $5.8 \text{ m}^3/\text{m}/\text{d}$ for fresh SGD (Table 6).

4.8. Radon surface water surveys and SGD flux scaling

While the radon time series provides a good estimate for average SGD over a tidal cycle, it does not provide information on the spatial distribution and heterogeneity of SGD. This can be studied by radon surface water survey SGD fluxes calculated at each field area. In Fig. 10, the multicolored lines indicate the path the boat traveled and the color gradient indicates the

Table 5

Time series model parameters and measurements. Time series locations, mixed salinity layer depths measured during depth profiling, surface area of radon model box, and shore parallel box side lengths are shown. The ^{222}Rn activity are mean values measured over an entire time series, while the standard deviations represent the tidally modulated variance that occurs over the duration of the time series.

Field area	Latitude	Longitude	Depth (cm)	Surface area (m ²)	Length of Shoreline (m)	Mean ^{222}Rn activity (dpm/L)
Kuau	20.92622	-156.37012	65	2568	105	11.6 ± 3.9
Maalaea	20.79177	-156.50947	75	4172	61	9.6 ± 3.1
Kahului	20.89699	-156.45493	99	1434	100	1.1 ± 0.6
Honolua	21.01325	-156.63942	35	414	41	9.0 ± 4.2
Waiehu	20.91541	-156.49156	63	4643	217	0.6 ± 0.2
Honomanu	20.86082	-156.16530	77	2507	108	6.1 ± 2.8

Table 6

Mean total and fresh SGD fluxes calculated from stationary radon time series data over a tidal cycle. For the fluxes, standard deviations are indicated after the ± symbol and represent the tidally modulated variance that occurs over the duration of the time series. The mean salinity of coastal groundwater (CGW) samples used to calculate the fresh SGD fraction is shown along with the standard deviation, and the number of samples used in the mean calculation are in parenthesis.

Field area	Mean total SGD flux (m ³ /m/day)	Mean CGW salinity	Fresh SGD flux (m ³ /m/day)
Kuau	5.1 ± 2.8	5.0 ± 6.1 (10)	4.4 ± 2.5
Maalaea	6.9 ± 3.4	22.2 ± 14.5 (12)	2.6 ± 1.3
Kahului	1.1 ± 0.4	8.2 ± 5.1 (9)	0.8 ± 0.3
Honolua	3.3 ± 1.9	4.9 ± 6.7 (10)	2.4 ± 1.4
Waiehu	1.1 ± 0.5	12.8 ± 12.7 (7)	0.7 ± 0.4
Honomanu	6.6 ± 6.1	4.1 ± 4.7 (8)	5.8 ± 5.4

Table 7

Radon surface water survey parameters and SGD fluxes. The mean and standard deviation for select parameters used in radon surface water survey SGD flux calculations as well as the calculated fluxes are shown. The standard deviation represents the variance that occurred along the entire survey at a particular area. The last column shows the mean ratio of the survey flux calculated for each coastal box relative to the survey flux calculated for the coastal box at the time series location.

Field Site	Sal.	Depth (m)	^{222}Rn activity (dpm/L)	SGD (m ³ /day)	SGD (m ³ /m/day)	Discharge relative to TS location
Kuau	34.35 ± 0.34	0.7 ± 0.2	3.0 ± 1.4	340 ± 260	2.3 ± 1.7	0.86 ± 0.68
Maalaea	33.60 ± 1.8	0.3 ± 0.3	9.2 ± 4.8	53 ± 74	0.5 ± 0.4	1.6 ± 1.9
Kahului	32.39 ± 0.45	1.6 ± 0.4	2.4 ± 1.0	450 ± 308	2.1 ± 1.6	1.4 ± 0.97
Honolua	34.82 ± 0.20	0.7 ± 0.7	1.0 ± 0.6	14 ± 16	0.1 ± 0.1	1.8 ± 2.0
Waiehu	31.91 ± 1.8	0.5 ± 0.3	0.7 ± 0.6	24 ± 29	0.2 ± 0.2	0.79 ± 1.0
Honomanu	32.00 ± 2.2	1.4 ± 0.5	3.1 ± 1.9	131 ± 57	0.6 ± 0.3	0.50 ± 0.15

Table 8

Scaled total and scaled fresh SGD rates at each of the field areas. Fluxes presented are mean flux calculated over a tidal cycle. Standard deviations are indicated after the ± symbol and represent the tidally modulated variance that occurs over the duration of the time series. The error is the propagated uncertainty associated with the calculated flux.

	Scaled total SGD (m ³ /m/d)	Error	Scaled fresh SGD (m ³ /m/d)	Error
Kuau	4.4 ± 2.4	1.1	3.8 ± 2.1	0.9
Maalaea	10.9 ± 5.4	5.2	4.1 ± 2.0	2.0
Kahului	1.5 ± 0.6	0.9	1.1 ± 0.5	0.7
Honolua	5.9 ± 3.3	0.7	4.4 ± 2.5	0.6
Waiehu	0.8 ± 0.4	0.8	0.5 ± 0.3	0.5
Honomanu	3.3 ± 3.1	1.4	2.9 ± 2.7	1.2

magnitude of SGD flux. Important parameters used in the SGD fluxes along with the calculated fluxes are shown in Table 7. Radon surface water survey SGD fluxes are used to scale the time series calculated fluxes. The mean ratio of the radon survey flux at every other location along each shoreline transit relative to the survey flux calculated at the time series location is included in Table 7. This mean ratio is multiplied by the mean SGD flux to determine the SGD flux scaled to a larger area. In the discussions that follow we further proportion these scaled time series flux rates (section 3.6.3) between total (fresh + marine) and freshwater only (Section 3.6.4) SGD fractions, and refer to them as either scaled total or scaled fresh SGD for the remainder of the text below.

4.9. SGD rates and nutrient fluxes

SGD fluxes calculated at the time series location and scaled SGD fluxes are shown in Fig. 11a and b, respectively, along with the uncertainty associated with the measurement. Nutrient fluxes for a particular field area are shown in Table 9 and determined by multiplying the groundwater endmember nutrient concentration (Table 3) by the scaled fresh SGD flux (Table 8). Uncertainties associated with the nutrient flux measurements are presented in Table 9. Nutrient fluxes for NH_4^+

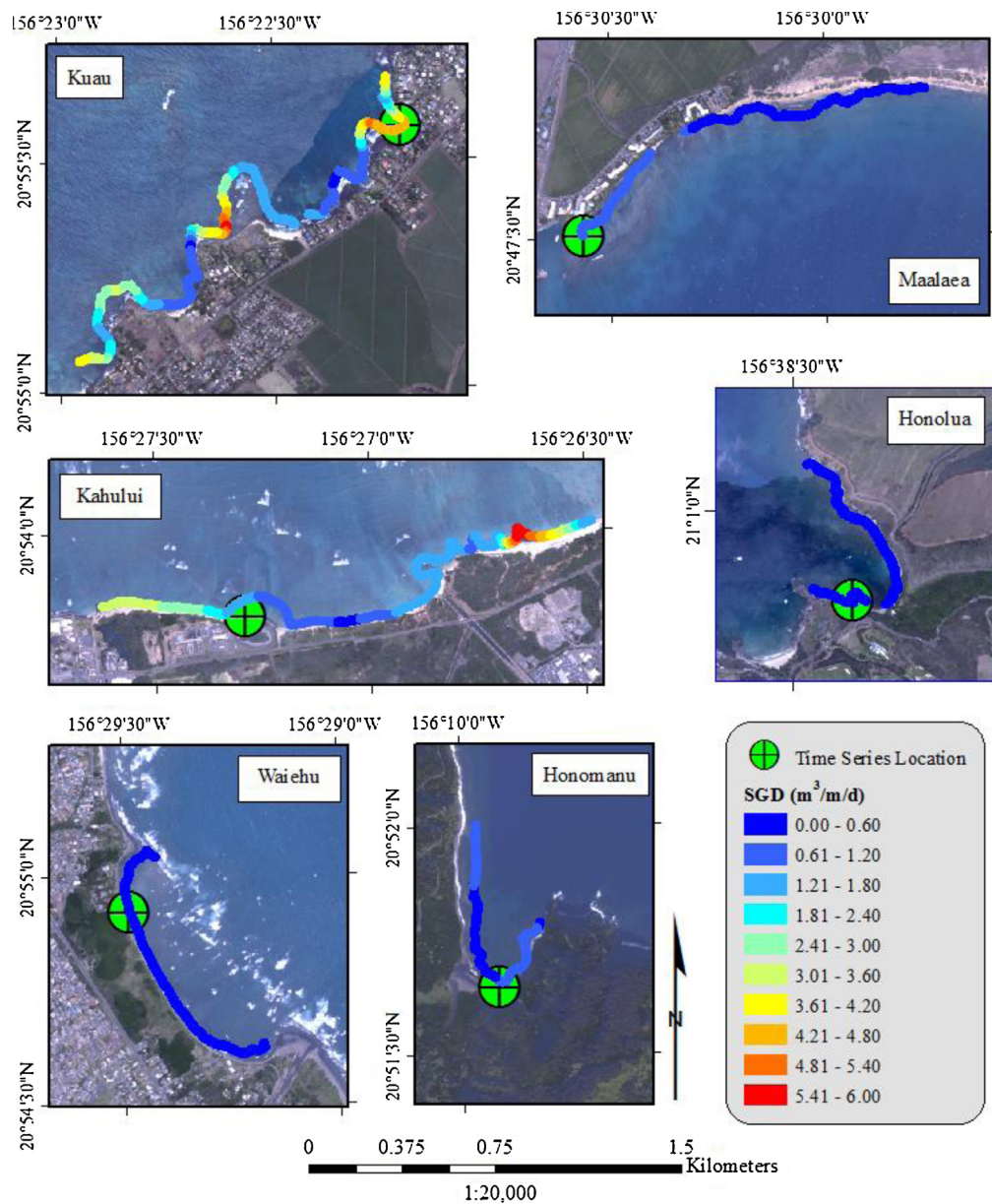


Fig. 10. Surface water radon survey fluxes. Total SGD fluxes ($\text{m}^3/\text{m}/\text{d}$) calculated from radon surface water surveys at each field area. Green circles indicate the locations of radon time series stations.

Table 9

Nutrient fluxes. Nutrient fluxes were determined for scaled fresh SGD rates. Standard deviations are indicated after the \pm symbol and represent the tidally modulated variance that occurs over the duration of the time series. The error is the propagated uncertainty associated with the calculated nutrient fluxes.

Field area	PO_4^{3-} (mmols/m/d)	Error	Si (mmols/m/d)	Error	N + N (mmols/m/d)	Error
Kuau	19 ± 10	5.4	3400 ± 1900	800	1700 ± 920	400
Maalaea	30 ± 14	14	2500 ± 1200	1200	1200 ± 580	590
Kahului	2.6 ± 1.2	1.7	730 ± 330	490	61 ± 28	44
Honolua	8.0 ± 4.5	1.6	2100 ± 1200	300	130 ± 73	30
Waiehu	1.3 ± 0.8	1.6	250 ± 150	250	18 ± 11	22
Honomanu	9.9 ± 9.2	5.0	2000 ± 1800	930	23 ± 21	11

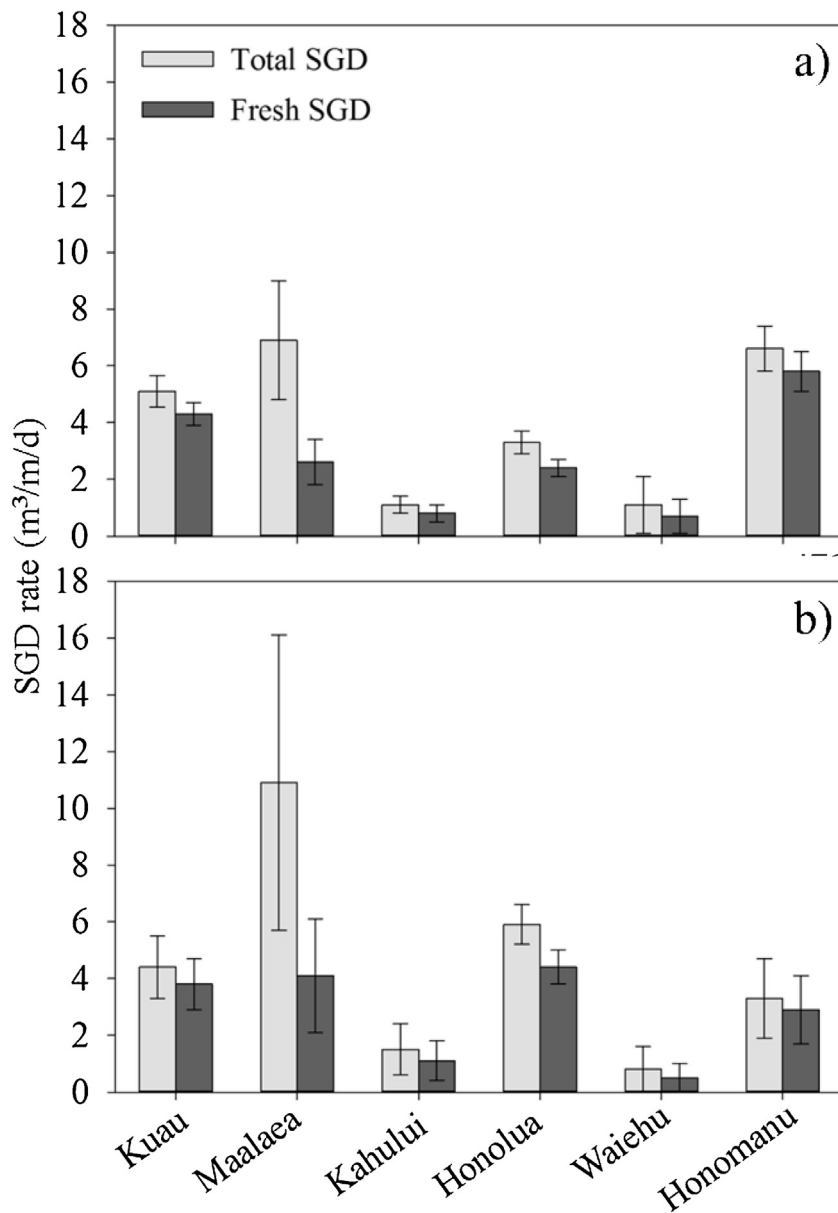


Fig. 11. SGD fluxes at each field area. Stationary time series fluxes (a) and scaled SGD fluxes (b). Error bars are the propagated uncertainty associated with the flux calculation.

were not calculated because of the large uncertainty associated with calculating the NH_4^+ endmember. For the purpose of this discussion, all references to nutrient fluxes will be in regard to the flux calculated using the scaled fresh SGD.

5. Discussion

5.1. Nutrient trends in groundwater and coastal waters

Ocean waters surrounding Hawai'i are oligotrophic and the majority of nutrients in coastal waters are supplied by terrestrial sources. Groundwater nutrient input is likely driving observed coastal water nutrient concentrations as evidenced by the fact that field areas with high groundwater endmember $\text{N} + \text{N}$ and Si concentrations also have high mean $\text{N} + \text{N}$ and Si coastal water concentration and vice-versa. Furthermore, $\text{N} + \text{N}$, PO_4^{3-} , and Si are significantly inversely linearly correlated with distance from shore at most field areas, again suggesting a terrestrial source. Coastal water nitrate is terrestrial in origin as evidenced by similarity between coastal water and coastal groundwater $\delta^{15}\text{N}$ and $\delta^{18}\text{O}$ values from a particular field area, except at Kahului, which is discussed below. During this study stream water was discharging at both Waiehu

and Honomanu and therefore stream input cannot be discounted as a source of nutrients at those sites. However, stream nutrient concentrations at these two sites were low, particularly for N + N (<2 μM) and coastal water nutrient concentrations were low relative to other areas, suggesting that neither streams nor groundwater are substantial sources of nutrients to coastal waters at these two sites. The four other areas studied did not have stream inputs and were not sampled during rain events so nutrient contribution from streams or runoff is unlikely, particularly because residence times measured on south Maui coastal waters, though not at our field sites, ranged between 1 and 6 h (Herzfeld, 2011). Tables 2 and 3 show that mean coastal water and groundwater endmember N + N concentrations vary considerably among the field areas, by factors of 383 and 55, respectively, while the other species vary by less than a factor of 5. The important implication of this result is that it suggests that land use has a substantial effect on N+N concentrations, and a much smaller effect on the other nutrient species.

The relatively little amount of variation in PO_4^{3-} concentrations is likely due to the highly reactive nature of PO_4^{3-} and the tendency of that nutrient species to sorb to aquifer materials, particularly iron oxides (Robertson et al., 1998; Benner et al., 2002; Santos et al., 2008). Because PO_4^{3-} has poor solubility and does not readily transport, measured PO_4^{3-} concentrations likely represent a localized input and not the integration of PO_4^{3-} from different types of land use over the entire length of a groundwater flowpath. Reducing conditions can indirectly increase the solubility of PO_4^{3-} by converting insoluble ferric iron to more soluble ferrous iron (Appelo and Postma, 2010) but for most samples collected during this study dissolved oxygen concentrations did not indicate that sampled groundwater was reducing. Furthermore, Hawaiian groundwaters are typically well oxygenated (Kelly, 2012) and thus the mobilization of PO_4^{3-} would not be expected.

The low variability in Si concentrations is likely due to the fact that Si in Hawaiian groundwater is nearly entirely derived from soil and rock weathering (Visher and Mink 1964; Vitousek, 2004 and references therein). Thus, differences in concentration among the field areas reflect the geology and soil type more than land use. It has been suggested that increased irrigation can accelerate weathering and leach more Si into groundwater (Visher and Mink, 1964; Tetra Tech Inc., 1994), although in this study no consistent trends were observed in Si concentrations collected from waters proximal to agricultural lands.

5.2. Application of multiple regression modeling to nutrient source identification

The results of our regression analysis of land use types (Table 4) suggests that for sites studied on Maui sugarcane contributes the greatest amount of N + N to groundwater, followed by pineapple. These results are consistent with the results from $\delta^{15}\text{N}$ values of dissolved nitrate, discussed below. In contrast, undeveloped land and unspecified agriculture have an inverse relationship with N + N. Data on undeveloped lands suggest a lack of anthropogenic sources to contribute N to groundwater in these areas. The inverse relationship between N + N and unspecified agriculture is difficult to explain but could be a result of nitrogen storage and removal in soil.

5.3. Sources of nutrients to the field areas

5.3.1. Undeveloped land (Honomanu)

The lowest N + N coastal groundwater endmember concentrations occurred at Honomanu Bay where groundwater flows beneath almost exclusively (99%) undeveloped land (Fig. 4). Coastal water N + N concentrations at Honomanu were also very low (Table 2) reflecting the low groundwater endmember concentration. Mean $\delta^{15}\text{N}$ and $\delta^{18}\text{O}$ isotopic compositions are also lowest at Honomanu, suggesting that the nitrite in this field area is primarily coming from soils or atmospheric deposition. Honomanu thus represents a baseline endmember by which N+N concentrations from other areas can be compared.

5.3.2. Commercial agriculture and OSDS (Kauai)

At Kauai, groundwater flowpaths are overlain by a number of different land use types (Fig. 4) including pineapple, sugarcane, and OSDS, making identification of nutrient sources difficult. To discriminate nitrate contributions in this area we examined changes in $\delta^{15}\text{N}$ values and nitrate concentration along groundwater flowpaths. Upslope of the Kauai coastal field area we sampled three public water supply wells (Fig. 12A). The groundwater hydraulic gradient is approximately perpendicular to elevation contours so groundwater flows roughly downhill. As shown in Fig. 12A, groundwater NO_3^- concentration increases down-gradient from 29 μM at KW to 94 μM at HW, while $\delta^{15}\text{N}_{\text{NO}_3}$ values are effectively unchanged. The increase in NO_3^- concentration occurs as groundwater transects land use that includes a large area with a high density of septic systems and lesser amounts of undeveloped land, developed land, and pineapple. Because $\delta^{15}\text{N}$ values do not change, the $\delta^{15}\text{N}$ of the 65 μM of added nitrate must also have a $\delta^{15}\text{N}$ of around 4‰. This value is consistent with values expected from soil, air, and fertilizer-derived nitrate, and too low for the 10–20‰ expected from an OSDS source (McMahon and Bohlke, 2006; Kendall, 1998). Further upslope, the PW well has a lower $\delta^{15}\text{N}$ value and thus there is an increase in $\delta^{15}\text{N}$ values from PW well to HW well. Assuming the 71 μM increase in NO_3^- is from a single source we can use a 2-component isotope mass balance to estimate the $\delta^{15}\text{N}$ value of the NO_3^- added:

$$94 * \delta^{15}\text{N}_{\text{HW}} = 23 * \delta^{15}\text{N}_{\text{PW}} + 71 * \delta^{15}\text{N}_{\text{added}} \quad (6)$$

where 94, 23, and 71 are the concentrations of NO_3^- at HW, PW, and HW–PW, respectively, $\delta^{15}\text{N}_{\text{HW}} = 4.0\text{‰}$, $\delta^{15}\text{N}_{\text{PW}} = 2.9\text{‰}$, and $\delta^{15}\text{N}_{\text{added}}$ is the isotopic composition of the NO_3^- added. Solving for $\delta^{15}\text{N}_{\text{added}}$ yields a value of $4.3 \pm 1.4 \text{‰}$, well below

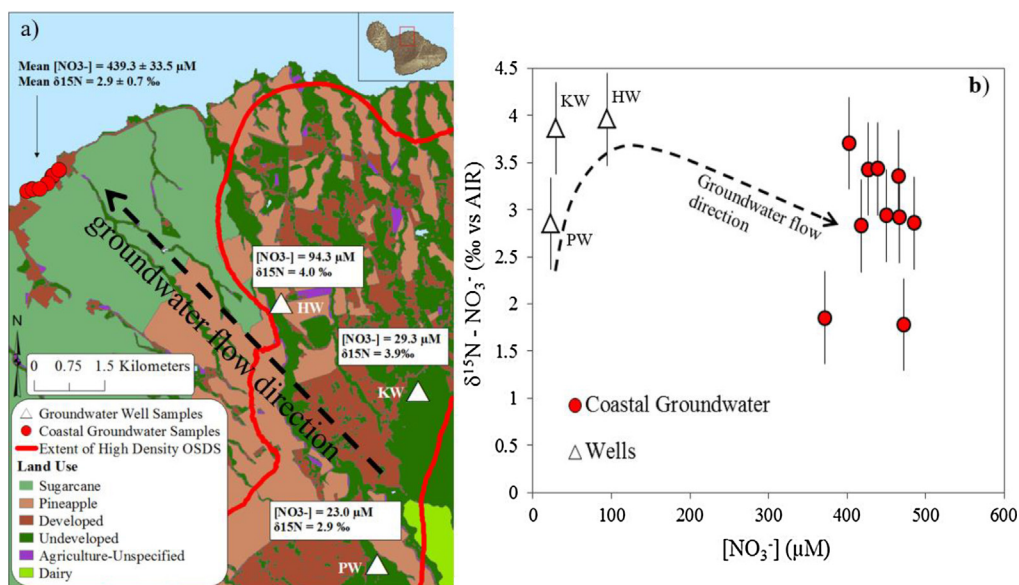


Fig. 12. Kuau nutrient sources. (a) Land use, sampling locations, approximate groundwater flow direction, $\delta^{15}\text{N}$ values, and nitrate concentrations. (b) Binary plot showing change in $\delta^{15}\text{N}$ and NO_3^- concentration along the groundwater flowpath.

the 10–20‰ value expected for OSDS nitrate. The important implication of these analyses is that while groundwater flows beneath this high density OSDS area, $\delta^{15}\text{N}$ values do not suggest that significant OSDS nitrate is added.

An examination of coastal groundwater samples at Kuau reveals that the mean NO_3^- concentration is $345 \mu\text{M}$ higher than the nearest upgradient well (HW; Fig. 12B). The increase in NO_3^- concentration between HW well and the coast occurs as groundwater leaves the high-density septic area and flows beneath pineapple and sugarcane fields (Fig. 12A). The $\delta^{15}\text{N}$ values decrease from well HW to the coast. Using a two component isotope mass balance equation we can estimate the $\delta^{15}\text{N}$ of the added NO_3^- :

$$439 \times \delta^{15}\text{N}_{\text{CGW}} = 94 \times \delta^{15}\text{N}_{\text{HW}} + 345 \times \delta^{15}\text{N}_{\text{added}} \quad (7)$$

where 439, 94, and 345 are the concentrations of mean coastal groundwater (CGW), HW, and the nitrate added from HW to CGW, $\delta^{15}\text{N}_{\text{CGW}} = 2.9\text{‰}$, $\delta^{15}\text{N}_{\text{HW}} = 4.0\text{‰}$, and $\delta^{15}\text{N}_{\text{added}}$ is the isotopic composition of the nitrate added. Solving for $\delta^{15}\text{N}_{\text{added}}$ yields a value of $2.6 \pm 1.1\text{‰}$. The urea fertilizer applied to sugarcane and pineapple fields (Falconer, 1991) converts to nitrate with a typical $\delta^{15}\text{N}$ value of around $0 \pm 1.3 \text{‰}$ and average soil nitrate $\delta^{15}\text{N}$ produced from fertilizer is 4.3‰ (Kendall, 1998; Böhlke, 2003). The $\delta^{15}\text{N}$ value calculated for the nitrate added is similar to the values of both urea derived nitrate and soil nitrate produced from fertilizer (Kendall, 1998). Thus, mixing of low $\delta^{15}\text{N}$ nitrate derived from urea fertilizers with background groundwater, which has a $\delta^{15}\text{N}$ of around 4.0‰ , is the likely explanation for the observed decrease in isotopic composition and $345 \mu\text{M}$ increase in nitrate concentration between the lowest elevation well and the coast. Although soils and the atmosphere can produce values around 2.6‰ , the large increase in nitrate concentration that occurs as groundwater flows beneath sugarcane and pineapple fields suggests a fertilizer source. Because nitrate comprises greater than 99% of the N + N concentration in each of the samples collected at Kuau we calculate that commercial agriculture is adding $\sim 78\%$ of the $440 \mu\text{M}$ coastal groundwater endmember N + N.

5.3.3. Appraisal of wastewater injection (Kahului)

5.3.3.1. Three endmember mixing analysis. The Kahului Wastewater Treatment Facility (KWWTF) injects approximately $15,000 \text{ m}^3$ of treated effluent per day (Scott Rollins, KWWTF, personal communication; Dailer et al., 2010) through eight injection wells less than 50 meters from the coast. Using $\delta^{18}\text{O}_{\text{H}_2\text{O}}$ values and salinity we conducted a two component, three endmember mixing analysis to determine if this effluent was present in coastal groundwater. Salinity and $\delta^{18}\text{O}_{\text{H}_2\text{O}}$ values are appropriate tracers for this kind of analysis because both exhibit conservative chemical behavior (Fig. 6) and all three endmembers have different concentrations and compositions for each of the tracers. In this model we assume that the chemical composition of the coastal groundwater samples is a combination of upland groundwater, coastal water, and injected effluent, whereby endmembers used in this analysis are water from the PW public drinking water supply well, the mean coastal water isotopic composition and salinity of all coastal water samples collected from coastal waters at Kahului ($n = 22$), and wastewater effluent obtained from the KWWTF. Fig. 13A illustrates how the nine Kahului coastal groundwater samples plot relative to these endmembers. Samples within the endmember triangle shown in Fig. 13A are comprised entirely of some proportion of these endmembers, while samples that plot outside the triangle cannot be satisfactorily explained by the model compositions alone. Five of the nine coastal groundwater samples collected at Kahului do not fall within the

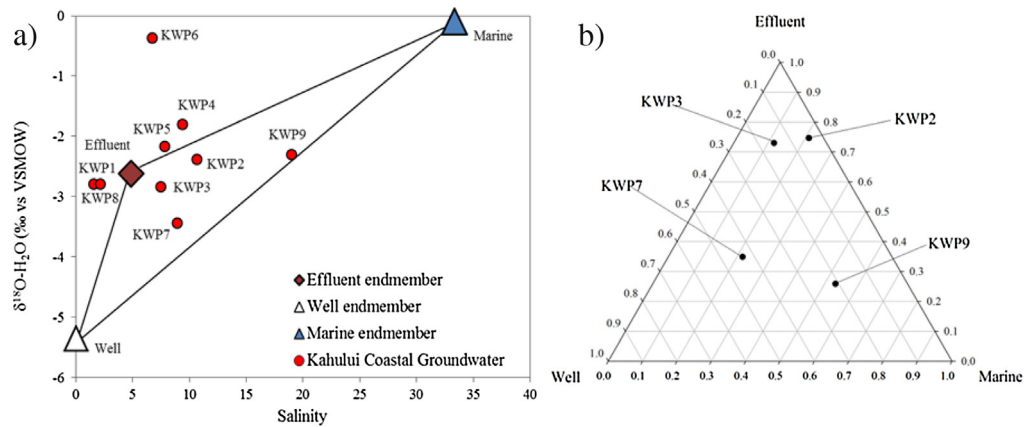


Fig. 13. Three-component mixing analysis of the contribution of wastewater injection to coastal groundwater. (a) The three component mixing model endmembers that mix to form Kahului coastal groundwater are the PW well (white triangle), mean marine surface water from Kahului (blue triangle) and Kahului Wastewater Treatment Facility effluent (red diamond). Red dots are coastal groundwater samples from the Kahului field area and sample names are shown. Black lines are conservative mixing lines between two of the end-members. Samples that plot within the mixing triangle are comprised entirely of some proportion of the three end-members while samples that plot outside do not fit in the model. (b) Ternary diagram shows the proportion of each endmember that mixed to form the coastal groundwater samples that lie within the mixing triangle from (a).

mixing triangle. However, because four of the five samples that plot outside the triangle plot are quite close to the triangle edges, and cluster around the effluent endmember, we suspect that the endmembers chosen are correct, but that the single effluent sample we are using as the effluent endmember is not capturing the full variability in chemical composition. Similar investigations of the Lahaina Wastewater Treatment Facility in west Maui (Hunt and Rosa, 2009; Glenn et al., 2012, 2013) for example, have shown that the $\delta^{18}\text{O}_{\text{H}_2\text{O}}$ values and salinity of the injected effluent is temporally variable and it is possible that the single sample is not completely representative of the bulk composition of effluent injected into the aquifer. The ternary diagram (Fig. 13B) is used to show the proportion of each endmember in a sample after calculating relative fractions. The fraction of each end member was calculated by simultaneously solving a system of three equations and three unknowns:

$$1 = f_m + f_{GW} + f_{eff} \quad (8)$$

$$S_{KWP} = S_m f_m + S_{GW} f_{GW} + S_{eff} f_{eff} \quad (9)$$

$$\delta^{18}\text{O}_{KWP} = \delta^{18}\text{O}_m f_m + \delta^{18}\text{O}_{GW} f_{GW} + \delta^{18}\text{O}_{eff} f_{eff} \quad (10)$$

where f is the fraction of each end-member, S is salinity, $\delta^{18}\text{O}$ is the oxygen isotope composition of water, the subscripts m , GW , and eff are for the marine, groundwater, and effluent end-members, respectively, and the subscript KWP is the sample being evaluated. The results of the mixing analysis using the PW well $\delta^{18}\text{O}$ values show that the four groundwater samples within the mixing triangle range in their end-member compositions from 12 to 53% marine, 4–44% upland groundwater, and 26–75% effluent (Fig. 13B).

5.3.3.2. N and O isotopic composition of dissolved nitrate. The $\delta^{15}\text{N}$ and $\delta^{18}\text{O}$ values of dissolved nitrate suggest wastewater effluent is discharging to groundwater and coastal water at Kahului. N and O isotopic composition of dissolved nitrate have been used extensively to identify sources and transformations of NO_3^- in groundwater and marine systems (Kendall, 1998; Böhlke, 2003; Singleton et al., 2005; McMahon and Böhlke, 2006; Wankel et al., 2006; Hunt and Rosa, 2009; Kaushal et al., 2011; Glenn et al., 2012; Lapworth et al., 2013). The sample of treated effluent collected from KWWTF had $\delta^{15}\text{N}$ and $\delta^{18}\text{O}$ values of 21.4‰ and 11.3‰, respectively, which are consistent with values expected for treated sewage and similar to effluent values measured at other municipal wastewater treatment facilities on Maui (Hunt, 2007; Hunt and Rosa, 2009; Glenn et al., 2012). The wastewater treatment process used at Kahului includes simultaneous nitrification-denitrification to attenuate N-species concentrations (County of Maui, 1990). This treatment ends after the denitrification phase, which leaves residual nitrate with $\delta^{15}\text{N}$ and $\delta^{18}\text{O}$ values that reflect the denitrification process. The samples from Kahului coastal groundwater and coastal surface waters had $\delta^{15}\text{N}$ values ranging from 7.0–44.1‰ (Fig. 7), with values on the high end of this range being consistent with nitrate-N that has been partially denitrified. Furthermore, many of the samples plot along a theoretical denitrification trend in which the isotopic enrichment of oxygen relative to nitrogen occurs in a ratio of approximately 1:2 (Kendall, 1998) (Fig. 7). This suggests that the nitrate in those samples have undergone partial denitrification, a phenomenon not observed in samples from any of the other field areas.

The $\delta^{15}\text{N}$ values observed in coastal groundwater samples collected from the Kahului field site bracket and cluster around the value of the effluent (Fig. 7), i.e., some values are lower and some are higher than the effluent. Samples with $\delta^{15}\text{N}$ values higher than the effluent sample contain nitrate that is derived from the wastewater injection facility but has continued to denitrify as it flowed through the aquifer, after injection. This process has been observed by Glenn et al. (2012,2013) near

Lahaina, Maui for coastal water samples clearly fed in large part by Maui County municipal wastewater injection wells. Our samples had NO_3^- concentrations that were low relative to other samples from Kahului (mean = 6.5 μM), as would be expected as a result of denitrification. By contrast, samples with $\delta^{15}\text{N}$ values lower than the effluent sample had NO_3^- concentrations that were generally higher (mean = 23.7 μM) than ^{15}N -enriched samples, as would be expected from nitrate that has either mixed with another source and/or undergone lesser amounts of denitrification. All the samples that fall within the three endmember mixing triangle (Fig. 13A) had $\delta^{15}\text{N}$ values that were lower than the effluent, suggesting a mixture of effluent with low $\delta^{15}\text{N}$ background groundwater is the reason for the $\delta^{15}\text{N}$ values lower than the effluent endmember. The land use transected by Kahului coastal groundwater is most similar to land use transected by Kuau and Honolua (Fig. 4), areas with mean $\delta^{15}\text{N}$ values of 2‰ and 3.5‰, respectively, thus it is reasonable to expect the background groundwater nitrate at Kahului to have values in that range. Therefore, a mixture of background groundwater with a $\delta^{15}\text{N}$ of 2‰ to 3.5‰ and effluent with a $\delta^{15}\text{N}$ of ~22‰ could produce the values between 7 and 22‰ observed in some samples. While the high $\delta^{15}\text{N}$ values do not singularly identify wastewater as the nitrate source (e.g., Houlton et al., 2006) values upwards of 14‰ were not measured in any samples collected during this study, except for the samples from Kahului. This suggests that processes that may drive $\delta^{15}\text{N}$ and $\delta^{18}\text{O}$ towards high values are uncommon on Maui except in the presence of wastewater effluent.

5.3.4. Commercial agriculture and local wastewater injection (Maalaea)

The most likely sources of nutrients to coastal waters at Maalaea are sugarcane, which comprise 94% of the land use transected by groundwater flowpaths in the area, and localized, relatively small volume (550 m^3/day) wastewater injection wells at some of the beachside condominiums (Dollar et al., 2011). Our data are inconsistent with the presence of wastewater effluent because groundwater and coastal water $\delta^{15}\text{N}$ values are low (mean $\delta^{15}\text{N}$ = 3.13 ‰), NH_4^+ concentrations are low (mean = 0.71 μM), and dissolved oxygen concentrations are high (mean >100%). We were unable to collect background groundwater sample at Maalaea or an effluent sample from the coastal injection wells but we assume mean background groundwater $\delta^{15}\text{N}$ values at Maalaea are similar to Kuau (3.3‰), which has the most similar land use (Fig. 3). We also assume that injection effluent $\delta^{15}\text{N}$ values at Maalaea condominiums are similar to that at Kahului wastewater treatment plant (21.38‰). If these assumptions are true, the mean $\delta^{15}\text{N}$ values of 3.13‰ at Maalaea could not occur as a result of mixing background groundwater with effluent.

The highest $\delta^{15}\text{N}$ value (4.6‰) at Maalaea could be a result of mixing effluent with background groundwater, but two component isotope mixing analysis suggests effluent is not present. Reported NO_3^- concentration of a near-coast irrigation well (well 4830-01; Dollar et al., 2011) is 190 μM . Salinity-unmixed NO_3^- concentration in the coastal groundwater sample with highest $\delta^{15}\text{N}$ (4.6‰) is 310 μM . Thus, we calculate the $\delta^{15}\text{N}$ of the 120 μM NO_3^- added to the groundwater system between the well and the coast as:

$$310 \times \delta^{15}\text{N}_{\text{sample}} = 190 \times \delta^{15}\text{N}_{\text{BG}} + 120 \times \delta^{15}\text{N}_{\text{added}} \quad (11)$$

where 310, 190, and 120 are the concentrations of the coastal sample, the well, and added nitrate and $\delta^{15}\text{N}_{\text{sample}} = 4.6$ ‰, $\delta^{15}\text{N}_{\text{BG}} = 3.3$ ‰, and $\delta^{15}\text{N}_{\text{added}}$ is the value of the added nitrate. In solving the equation we find $\delta^{15}\text{N}_{\text{added}}$ is 7.0 ± 3.4 ‰, which is much lower than the values measured in effluent from the three Maui wastewater treatment facilities, which ranged from 14.7–31.5 ‰ (Hunt, 2007; Hunt and Rosa, 2009; Glenn et al., 2012). This suggests that injected wastewater is not a substantial component of SGD discharging to Maalaea coastal waters. The $\delta^{15}\text{N}$ of the 120 μM of added nitrate is at the higher end of values reported for fertilizers, though near the middle of the range of values reported for fertilized soils (Kendall, 1998). Thus, the high N+N concentrations observed at Maalaea are predominantly from fertilizers applied to sugarcane, which overlies nearly the entire length of the groundwater flowpaths.

5.3.5. OSDS (Waiehu)

Waiehu has been identified as being at high risk from OSDS contamination to groundwater and coastal waters (Whittier and El-Kadi, 2014) and is the only field area other than Kahului that had elevated nitrate $\delta^{15}\text{N}$ values, which is suggestive of septic nitrate. Land use, groundwater flowpaths, wells, coastal samples, spring samples, $\delta^{15}\text{N}$ values, and NO_3^- concentrations for the area are detailed in Fig. 14A. Waiehu Bay is flanked by the Paukūkalo marsh, shown in Fig. 14A as a dark green sliver of undeveloped land. Coastal groundwater samples were collected along the beach on the seaward side of the marsh and two springs on the landward edge of the marsh. The N+N concentrations measured in groundwater samples from the beach were low, ranging from below detection to 3.2 μM . By contrast the springs on the landward side of the marsh had N+N concentrations of 58.7 and 103.2 μM . Upslope wells varied in N+N concentration from 10.6 to 33.0 μM . Salinity unmixed $\delta^{18}\text{O}_{\text{H}_2\text{O}}$ values in Waiehu coastal samples were more negative than the values of some of the upslope wells, suggesting that the groundwater in the coastal samples was recharged at an elevation equal to or greater than the upslope wells. We suspect that the Paukūkalo marsh may act a coastal “nutrient filter” that reduces the flux of N to the coast (e.g., Fisher and Acreman, 2004; Nelson and Zavaleta, 2012), perhaps due to biological N uptake by marsh plants, nitrate reduction within reducing marsh sediments, or other mechanisms. Whatever the mechanism, this apparently results in low observed nutrient concentrations in beachface and coastal water samples relative to spring samples collected from the landward edge of the marsh. Using a two component isotope mass balance calculation we can determine if the $\delta^{15}\text{N}$ value of nitrate in groundwater reflects an OSDS source. For this calculation we will ignore coastal samples as their chemistry appears to be affected

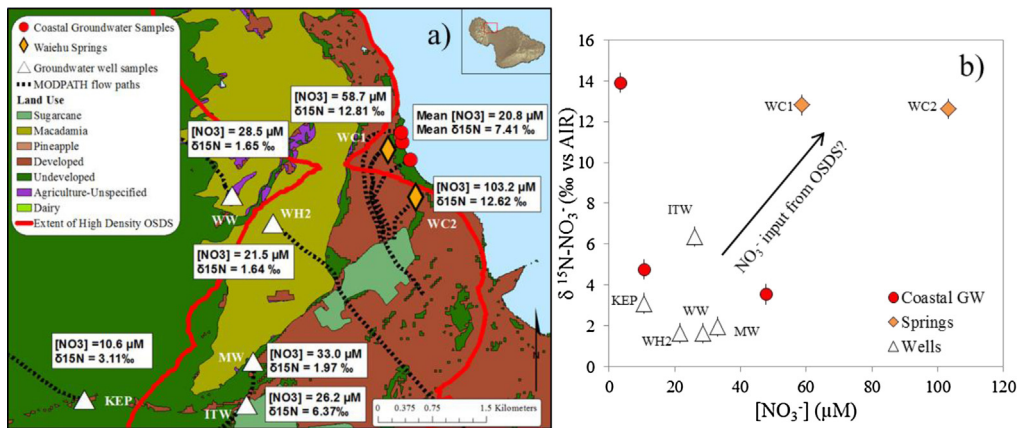


Fig. 14. Waiehu nutrient sources. (a) Land use, groundwater flowpaths, wells, springs, coastal samples, $\delta^{15}\text{N}_{\text{NO}_3}$ values, and NO_3^- concentrations. (b) Binary plot of $\delta^{15}\text{N}_{\text{NO}_3}$ vs NO_3^- concentration for Waiehu samples.

by the marsh and assume well WW represents the upslope groundwater endmember. We also assume nitrate added to groundwater is the difference between that of the spring samples and well WW. Thus:

$$81.0 \times \delta^{15}\text{N}_{\text{sample}} = 28.5 \times \delta^{15}\text{N}_{\text{WW}} + 52.5 \times \delta^{15}\text{N}_{\text{added}} \quad (12)$$

where 81.0, 28.5, and 52.5, are the mean coastal groundwater nitrate concentration, WW well nitrate concentration, and concentration of the added nitrate, respectively. $\delta^{15}\text{N}_{\text{sample}}$ is the mean $\delta^{15}\text{N}$ value of the spring samples (12.7‰), $\delta^{15}\text{N}$ is the WW well value (1.7‰), and $\delta^{15}\text{N}_{\text{added}}$ is the value of the added nitrate. Solving Eq. (12), we find $\delta^{15}\text{N}_{\text{added}} = 18.7 \pm 4.4\%$ which is within the 10–20‰ range of values reported for OSDS nitrate. It should be noted that the high $\delta^{15}\text{N}$ value calculated for the added nitrate could also be a result of denitrification, though we feel that this is unlikely for two reasons. First, $\text{NO}_2^-:\text{NO}_3^-$ is less than 0.1 for all samples and second, dissolved oxygen concentrations are above 80% in all samples except two. Both of these measurements suggest that redox conditions were not favorable for denitrification to occur. The mass balance suggests that approximately 50 μM of OSDS derived nitrate is being added to groundwater in Waiehu on the landward side of the Paukūkalo marsh. But, because N + N concentrations in coastal samples are lower than the springs, it appears that much of the OSDS nitrate in groundwater measured at the springs is being lost prior to reaching the coast. Furthermore, the $\delta^{15}\text{N}$ values in two of the three coastal samples are less than 5‰, which is not consistent with nitrate from an OSDS source. Although OSDS nitrate appears to be added to groundwater in Waiehu, the nutrients in that groundwater may be buffered by the marsh before reaching the coast, resulting in low coastal water nutrient impact. This scenario is a good example of the well-described ecosystem services that coastal wetlands provide (Mann, 2000).

5.4. SGD rates and nutrient fluxes

In Table 10 we present total and fresh SGD water and nutrient fluxes in order to compare them to the fluxes measured in other studies in Maui and elsewhere in Hawai'i. Our total SGD nutrient fluxes were calculated by multiplying the scaled total SGD flux by the mean nutrient concentration measured in all coastal groundwater samples from a particular area. The difference between total and fresh SGD nutrient is small. This is because fresh SGD nutrient fluxes have relatively low water discharge with high nutrient concentrations, whereas total SGD nutrient fluxes have relatively high discharge and lower (more dilute) nutrient concentration. We believe that our rates are conservative as we assigned a minimum box size based on shore parallel radon surveys and the time series location. The width of the coastal box used in the model was defined by radon survey data collected at the time series location, which we believe provides a reasonable estimate of SGD plume width. The maximum seaward length of the box was defined by the time series location. Although the SGD plume extent may have reached farther offshore than the time series location, we did not have the data required to determine the full seaward extent of the plume and concluded that a conservative estimate using the time series location is justified. Our SGD rates and nutrient fluxes presented here should be viewed as first order approximations because of the various assumptions inherent in the application of radon box models (Burnett and Dulaiova 2003; Dulaiova et al., 2010; Swarzenski et al., 2013) and because of uncertainties regarding seasonal variability. The highest N + N fluxes calculated in this study occur at Kuau where, based on N isotopic composition changes along a groundwater flowpath, we concluded that ~78% of coastal groundwater N + N is from fertilizers applied to commercial agriculture. As such, of the 1666 mmol/m/d of N + N that discharge to the coast at Kuau (Table 10), approximately 1300 mmol/m/d (78%) is from commercial agriculture and the remaining 366 mmol/m/d (22%) from other sources. At Maalaea we estimate that, based on $\delta^{15}\text{N}_{\text{NO}_3}$ values and the land use that groundwater flowpaths travel beneath, nearly all of the approximately 1190 mmol/m/d of N + N discharging to coastal water via SGD is from fertilizers applied to sugarcane fields. At Honomanu, where groundwater flowpaths traveled almost entirely undeveloped land, N + N flux was 23 mmol/m/d. Importantly, we find that the fertilizer-derived N + N fluxes

Table 10

Comparison of SGD and associated nutrient fluxes in this study to past studies in the Hawaiian Islands. Because most previous work calculated nutrient fluxes for total SGD, we present total SGD nutrient fluxes in addition to fresh SGD nutrient fluxes.

Site	Fresh SGD (m ³ /m/d)	Fresh PO ₄ ³⁻ flux (mmols/m/d)	Fresh Si flux (mmols/m/d)	Fresh N + N flux (mmols/m/d)
Kuau	3.8	19	3361	1666
Maalaea	4.1	30	2506	1192
Kahului	1.1	2.6	730	61
Honolua	4.4	8	2081	128
Waiehu	0.5	1.3	252	18
Honomanu	2.9	9.9	1974	23
Site and Study	Total SGD (m ³ /m/d)	Total PO ₄ ³⁻ flux (mmols/m/d)	Total Si flux (mmols/m/d)	Total N + N flux (mmol/m/d)
Kuau	4.4	19	3345	1660
Maalaea	11	50	4220	2072
Kahului	1.5	2.8	745	42
Honolua	5.9	9.1	2390	145
Waiehu	0.8	2.5	283	18
Honomanu	3.3	10	1952	21
Honolua, Maui ^d	2.5–21	1.2–8.7	–	6.2–72
Kahana, Maui ^{d,a}	4.2–11	3.6–9.0	–	144–360
Kahana, Maui ^{d,b}	250–530	200–430	–	8220–18000
Kahana, Maui ^e	35–113	–	–	1968
Mahinahina, Maui ^d	3.5–10	3–7.5	–	1840–6650
Honokowai, Maui ^d	2.7–7.2	0.5–9.0	–	54–153
Kahekili, Maui ^{e,f}	21–55	90–1400	6980–32000	1400–4700
Kahekili, Maui ^{e,g}	6–92	–	–	–
Hanalei, Kauai ^h	3.7–11	1.0–3.0	169–361	20–73
Haena, Kauai ^h	1.8–3.8	0.8–0.9	207–259	6.4–26
Kiholo, Hawai'i ⁱ	34	150	24900	6400

^a Calculated using 1.56 day residence time.

^b Calculated using 0.6 h residence time.

^c Fluxes were measured at springs discharging injected effluent and may be high due to the increased hydraulic gradient as a result of injection and high dissolved nutrient loads of the effluent.

^d Street et al. (2008).

^e Paytan et al. (2006).

^f Swarzenski et al. (2012).

^g Glenn et al. (2012, 2013).

^h Knee et al. (2008).

ⁱ Johnson (2008).

at Kuau and Maalaea are more than 50 times higher than the N + N flux from the relatively pristine Honomanu areas, despite the fact that fresh discharge at Kuau and Maalaea are only 1.3 and 1.4 times higher than Honomanu, respectively. At Kahului, where wastewater is discharging to groundwater and coastal water, the N + N flux is approximately three times higher than at Honomanu, yet still 19 times less than the fertilizer impacted N + N flux from Kuau. These findings imply that land use, particularly commercial agriculture, can exert a substantial impact on local coastal SGD nutrient flux.

In order to compare our results to the nutrient fluxes of streams and rivers, we upscale the nutrient flux to the ocean for each field area by multiplying the fresh SGD nutrient flux per meter of shoreline by the length of shoreline transected by the radon survey (Fig. 10). We compare our fluxes to two west Maui ephemeral streams and also to the two largest rivers in the state, the Wailuku and Hanalei Rivers. Total dissolved nitrogen flux for the West Maui streams was between 78 and 390 mols/d (Soicher and Peterson, 1997). Thus, at Maalaea and Kuau, where the majority of N is from sugarcane and pineapple fields, the N flux to the ocean is as much as 62 times greater than those from the west Maui streams. The Hanalei River on north Kauai delivers 544,000 m³/d of fresh water and an estimated 800 mols/d of N + N, 137 mols/d PO₄³⁻, and 114,667 mols/d Si (Knee et al., 2008). The SGD N + N flux is six and two times greater at Kuau and Maalaea, respectively, than the N + N flux from the Hanalei River even though the fresh SGD flux from these Maui sites are at most 5% of the Hanalei River discharge. SGD Si and PO₄³⁻ fluxes are lower than the Hanalei River fluxes, but still high for the amount of fresh SGD that discharges relative to riverine discharge. The Wailuku River in east Hawai'i island delivers an estimated 170,000 m³/d of fresh water during baseflow conditions and on average 660 mols/d of N + N, though during storms fresh discharge and nutrient flux can be five to ten times higher (Weigner et al., 2009). Similarly, SGD at Kuau and Maalaea delivers N + N loads that are eight and three times higher, respectively, than those delivered by the Wailuku River during baseflow conditions despite the fact that fresh SGD volumes are small (<7%) relative to the river discharge volume. Based on isotope mass balance, 3800 moles/d of N + N discharges to the Kuau field area from fertilizers applied to commercial agriculture, which is more than four times the amount of N + N discharged to coastal waters from either of the two largest rivers in the State. It is apparent that SGD N + N fluxes in areas impacted by land use can be substantially larger than the N fluxes from the State's two largest rivers, while SGD N + N fluxes from areas where land use has less impact are much smaller than riverine input (Table 11).

Table 11

Upscaled SGD rates and nutrient fluxes. Fresh SGD and associated nutrient fluxes are presented at each field area after upscaling by the length of shoreline transected by the radon survey. River and stream discharge rates and nutrient fluxes are also shown.

Field Area	Length (m)	Upscaled fresh discharge (m ³ /d)	PO ₄ ³⁻ (mols/d)	Si (mols/d)	N + N (mols/d)
Kuau	2946	11200	55	9902	4909
Maalaea	1568	6430	46	3930	1869
Kahului	2754	3030	7	2011	167
Honolua	1061	4670	8	2209	135
Waiehu	1252	626	2	316	23
Honomanu	1043	3020	10	2059	24
Stream/River	Island	Discharge (m ³ /d)	PO ₄ ³⁻ (mols/d)	Si (mols/d)	N + N (mols/d)
Honokowai ^b	Maui	–	–	–	390 ^a
Honokohua ^b	Maui	–	–	–	98
Hanalei ^c	Kaua'i	544000	140	114600	800
Wailuku ^d	Hawai'i	168000	–	–	660

^a Measured total dissolved nitrogen, not N + N.

^b Soicher and Peterson (1997).

^c Knee et al. (2008).

^d Weigner et al. (2009).

6. Conclusions

In this study we employed a combined methodology to determine the source, transport, and delivery rate of nutrients to the ocean via submarine groundwater discharge on Maui, HI. By combining groundwater and geochemical modeling with stable isotope analysis we are able to successfully connect land use practices along groundwater flowpaths with the nutrient fluxes to the ocean at the end of those flowpaths. Multiple regression and $\delta^{15}\text{N}$ values both suggest that commercial agriculture, particularly sugarcane, contributes the greatest amount of N + N to the ocean via SGD. Groundwater travel times in Hawai'i can occur on decadal time scales (Kelly and Glenn, 2015), thus the N+N from sugarcane and pineapple measured during this study likely represent both present and past contributions. Because sugarcane and, to a lesser extent pineapple, persist on Maui and because groundwater travel times on Maui are slow, the N + N flux from these agricultural practices will likely continue, even after production stops.

Our analysis of the Waiehu, Kuau, and Maalaea areas, where there is moderate to high risk of OSDS contamination to groundwater (Whittier and El-Kadi, 2014) or small-scale wastewater injection, showed mixed results in terms of identifying OSDS or wastewater derived nitrate. This may be because OSDS or wastewater nitrate is not identifiable with the applied tools in groundwater near Kuau or Maalaea or that $\delta^{15}\text{N}$ values are not always sufficient in identifying OSDS or wastewater nitrate. $\delta^{15}\text{N}$ values could be used to identify OSDS nitrate in groundwater near Waiehu where there is high OSDS risk, although the amount of N + N was relatively small. Similarly, $\delta^{15}\text{N}$ values suggest effluent discharges to groundwater and coastal water near Kahului where large volumes of wastewater are injected, but N + N fluxes and concentrations at Kahului at our study site are fairly low. Although N + N contributions from OSDS and wastewater appear to be low at these locations, the presence of OSDS and effluent is of concern because these waste sources may contribute bacteria, heavy metals, pharmaceuticals or other contaminants to groundwater and coastal water (Al-Bahry et al., 2014).

This work demonstrates that even though SGD water volume fluxes are much smaller, the coastal SGD N fluxes delivered from areas impacted by land use can be substantially larger than the N fluxes delivered by the State of Hawai'i 's two largest rivers. The large variation in N + N fluxes among the field areas studied is primarily a result of the differences in groundwater endmember N+N concentration; whereas fresh water SGD flux varied by a factor of only eight between areas with the lowest and highest discharge, the fresh water N+N concentration and resultant N + N flux varied by a factors of 55 and 92, respectively. At areas such as Kuau and Maalaea where there was a high fresh SGD flux and high groundwater nutrient endmember nutrient concentration, the risk of nutrient pollution by SGD is substantial. Thus, both groundwater endmember nutrient concentrations and fresh SGD flux must be considered when assessing coastal water nutrient pollution vulnerability in Hawai'i.

Acknowledgments

We would like to thank R. Peterson and an anonymous reviewer for their critical and detailed reviews of the manuscript. We also thank Brian Popp, Aly El-Kadi, Robert Whittier, Celia Smith, and Joseph Fackrell for enlightening discussions and constructive comments on this work, and for reviewing an earlier draft of the paper. We are indebted to Joe Fackrell, Chris Shuler, Sam Wall, and Jeff Skrotzki for their help and toil with fieldwork. We also thank Russell Sparks from the Maui Division of Aquatic Resources, Joe Mendonca from the Maui Department of Water Supply, Napua Barrows from the Waiehee Limu Restoration Project, and Maui Land and Pineapple Company, Inc., for logistic support. We thank the Geological Society of America for the Graduate Student Research Grant. This research was funded by a grant/cooperative agreement to Craig R. Glenn from the National Oceanic and Atmospheric Administration, Project R/HE-17, which is sponsored by the University of Hawai'i Sea Grant College Program, SOEST, under Institutional Grant No. NA09OAR4170060 from NOAA Office of Sea Grant,

Department of Commerce. The views expressed herein are those of the authors and do not necessarily reflect the views of NOAA or any of its subagencies. UNIHI-SEAGRANT-JC-13-32. This publication is University of Hawai'i School of Ocean and Earth Science and Technology Contribution Number 9519.

References

- Al-Bahry, S.N., Mahmoud, I.Y., Paulson, J.R., Al-Musharafi, S.K., 2014. Survival and growth of antibiotic resistant bacteria in treated wastewater and water distribution system and their implication in human health: a review. *Int. Arab. J. Antimicrob. Agents* 4 (2014), 1–11, <http://dx.doi.org/10.3823/758>.
- Appelo, C.A.J., Postma, D., 2010. *Geochemistry, Groundwater, and Pollution*, 2nd Ed. CRC Press, Taylor and Francis Group, Leiden, The Netherlands, 649 p.
- Benner, S.G., Hansel, C.M., Wielinga, B.W., Barber, T.M., Fendorf, S., 2002. Reductive dissolution and biomineralization of iron hydroxide under dynamic flow conditions. *Environ. Sci. Technol.* 38, 1705–1711.
- Berry, W.D., Feldman, S., (1985). Multiple regression in practice. Sage University Paper, series on Quantitative Applications in the Social Science, series 07-050. London.
- Böhlke, J.-K., (2003). Sources, transport, and reaction of nitrate. in: Lindsey, B.D., Phillips, S.W., Donnelly, C.A., Speiran, G.K., Plummer, L.N., Böhlke, J.-K., Focazio, M.J., Burton, W.C., Busenberg, E., (Eds.) Residence times and nitrate transport in ground water discharging to streams in the Chesapeake Bay Watershed: U.S. Geological Survey Water-Resources Investigations Report 03-4035, p. 25–39. <http://pa.water.usgs.gov/reports/wrir03-4035.pdf>.
- Borah, D.K., Bera, M., 2004. Watershed-scale hydrologic and nonpoint-source pollution models: review of applications. *ASAE* 47, 789–803, <http://dx.doi.org/10.13031/2013.16110>.
- Burnett, W.C., Dulaiova, H., 2003. Estimating the dynamics of groundwater input into the coastal zone via continuous radon-222 measurements. *J. Environ. Radioact.* 69, 21–35, [http://dx.doi.org/10.1016/S0265-931X\(03\)00084-5](http://dx.doi.org/10.1016/S0265-931X(03)00084-5).
- Burnham, W.L., Larson, S.P., Cooper, H.H.J., (1977). Distribution of injected wastewater in the saline lava aquifer, Wailuku-Kahului wastewater treatment facility, Kahului, Maui, Hawai'i. Open-file Report 77-469. <http://pubs.er.usgs.gov/publication/ofr77469>.
- Casciotti, K.L., Sigman, D.M., Hastings, M.G., Böhlke, J.K., Hilbert, A., 2002. Measurement of the oxygen isotopic composition of nitrate in seawater and freshwater using the denitrifier method. *Analyt. Chem.* 74, 4908–4912, <http://dx.doi.org/10.1021/ac020113w>.
- Cesar, S.F., van Beukering, P. J. H., (2004). Economic valuation of the coral reefs of Hawai'i. *Pac. Sci.* 58, pp. 231–242. <http://scholarspace.manoa.hawaii.edu/bitstream/handle/10125/2723/vol58n2-231-242.pdf?sequence=1>. 10.1353/psc.2004.0014.
- County of Maui, Department of Public Works, (1990). Environmental assessment and negative declaration for the Wailuku-Kahului wastewater reclamation facilities additions and modifications. <http://oeqc.doh.hawaii.gov/Shared%20Documents/EA.and.EIS.Online.Library/Maui/1990s/1990-12-08-MA-FEA-WAILUKU-KAHULUI-WASTEWATER-RECLAMATION.pdf>.
- Dailer, M.L., Knox, R.S., Smith, J.E., Napier, M., Smith, C., 2010. Using *N* values in algal tissue to map locations and potential sources of anthropogenic nutrient inputs on the island of Maui, Hawaii, USA. *Mar. Pollut. Bull.* 60, 655–671, <http://dx.doi.org/10.1016/j.marpolbul.2009.12.021>, http://coralreefecology.ucsd.edu/files/2010/09/Dailer_et-al_2010_MPB.pdf.
- Dailer, M.L., Smith, J.E., Smith, C.M., 2012. Responses of bloom forming and non-bloom forming macroalgae to nutrient enrichment in Hawai'i, USA. *Harmful Algae* 17, 111–125, <http://dx.doi.org/10.1016/j.hal.2012.03.008>.
- Dollar, S., Andrews, C., 1997. *Alga L Blooms off West Maui: Assessing Causal Linkages Between Land and the Coast Ocean*. University of Hawai'i at Manoa, Final Report, 40 p.
- Dollar, S., Atkinson, M., Hochberg, E., Nance, T., (2011). An evaluation of causal factors affecting coral reef community and benthic structure in Maalaea Bay, Maui, Hawai'i. Final report of the Maalaea Bay Coral Reef Degradation Study prepared for the county of Maui, 84 p. <http://hi-mauicounty.civicplus.com/DocumentCenter/View/83262>.
- Dulaiova, H., Peterson, R., Burnett, W.C., Lane-Smith, D., 2005. A multi-detector continuous monitor for assessment of ²²²Rn in the coastal ocean. *J. Radioanal. Nucl. Chem.* 263, 361–365, <http://dx.doi.org/10.1007/s10967-005-0063-8>.
- Dulaiova, H., Camilli, R., Henderson, P.B., Charette, M.A., 2010. Coupled radon, methane and nitrate sensors for large-scale assessment of groundwater discharge and non-point source pollution to coastal waters. *J. Environ. Radioact.* 101, 553–563, <http://dx.doi.org/10.1016/j.jenvrad.2009.12.004>.
- Engott, J.A., Vana, T.T., (2007). Effects of agricultural land-use changes and rainfall on groundwater recharge in central and west Maui, Hawai'i, 1926–2004. USGS Scientific Investigation Report, 2007–5103. <http://pubs.usgs.gov/sir/2007/5103/sir2007-5103-20pdf>.
- Falconer, J.K., 1991. Sugarcane fertilization practices on the Island of Maui. In: *Proceedings of the 50th Annual Conference of Sugarcane Technologists*, Honolulu, HI, November 11–13, pp. A-22–A-24.
- Fisher, J., Acreman, M.C., 2004. Wetland nutrient removal: a review of evidence. *Hydrol. Earth Syst. Sci.* 8, 673–685, <http://www.hydrol-earth-syst-sci.net/8/673/2004/hess-8-673-2004pdf>.
- Giambelluca, T.W., Chen, Q., Frazier, A.G., Price, J.P., Chen, Y.-L., Chu, P.-S., Eischeid, J.K., Delparte, D.M., (2011). The Rainfall Atlas of Hawai'i, Final Report. <http://rainfall.geography.hawaii.edu>.
- Giambelluca, T.W., Chen, Q., Frazier, A.G., Price, J.P., Chen, Y.-L., Chu, P.-S., Eischeid, J.K., Delparte, D.M., 2013. Online rainfall atlas of Hawai'i. *B. Am. Meteor. Soc.* 94, 313–316, <http://dx.doi.org/10.1175/BAMS-D-11-00228.1>.
- Gingerich, S.B., (2008). Ground-water availability in the Wailuku area, Maui, Hawai'i. USGS Scientific Investigations Report 2008–5236.
- Glenn, C.R., Whittier, R.B., Dailer, M.L., Dulaiova, H., El-Kadi, A.I., Fackrell, J., Kelly, J.L., Waters, C.A., (2012). Lahaina groundwater tracer study—Lahaina, Maui, Hawai'i. Final Interim Report. Prepared for the State of Hawai'i Department of Health, the U.S. Environmental Protection Agency, and the U.S. Army Engineer Research and Development Center, 463p. <http://www.epa.gov/region9/water/groundwater/uic-pdfs/lahaina02/lahaina-final-interim-report.pdf>.
- Glenn, C.R., Whittier, R.B., Dailer, M.L., Dulaiova, H., El-Kadi, A.I., Fackrell, J., Kelly, J.L., Waters, C.A., Sevadjian, J., (2013). Lahaina groundwater tracer study—Lahaina, Maui, Hawai'i, Final Report. Prepared for the State of Hawai'i Department of Health, the U.S. Environmental Protection Agency, and the U.S. Army Engineer Research and Development Center, 502p. <http://www.epa.gov/region9/water/groundwater/uic-pdfs/lahaina02/lahaina-gw-tracer-study-final-report-june-2013.pdf>.
- Granger, J., Sigman, D.M., Prokopenko, M.G., Lehmann, M.F., Tortell, P.D., 2006. A method for nitrite removal in nitrate N and O isotope analyses. *Limnol. Oceanogr.: Meth.* 4, 205–212.
- Harbaugh, A.W., (2005). MODFLOW-2005, The U.S. Geological Survey modular ground-water model—the ground-water flow process. U.S. Geological Survey Techniques and Methods 6-A16. <http://pubs.usgs.gov/tm/2005/tm6A16/>.
- Herzfeld, I., (2011). Physical regulation of land-ocean CNP flux and relationships to macroalgae blooms across coastal zones of Maui. Ph.D. Dissertation from the Department of Oceanography, Honolulu Hawai'i: University of Hawai'i at Manoa, 252p.
- Houlton, B.Z., Sigman, D.M., Hedin, L.O., 2006. Isotopic evidence for large gaseous nitrogen losses from tropical rainforests. *Proc. Natl. Acad. Sci.* 103, 8745–8750, <http://www.ncbi.nlm.nih.gov/pubmed/16728510>.
- Hunt, C.D., Jr., (2007). Ground-water nutrient flux to coastal waters and numerical simulation of wastewater injection at Kihei, Maui, Hawai'i: U.S. Geological Survey Scientific Investigations Report 2006–5283, 69p. <http://pubs.usgs.gov/sir/2006/5283/>.
- Hunt, C.D., Rosa S.N., (2009). A multitracer approach to detecting wastewater plumes at Kihei and Lahaina, Maui, Hawai'i. USGS Scientific Investigations Report 2009–5253, 166p. <http://pubs.usgs.gov/sir/2009/5253/>.
- Johnson, A.G., 2008. Groundwater discharge from the leeward half of the Big Island of Hawai'i. M.S. Thesis, Department of Geology and Geophysics. University of Hawai'i at Manoa, Honolulu Hawai'i, pp. 145p.

- Johnson, A.G., Engott, J.A., Bassiouni, M., (2014). Spatially distributed groundwater recharge estimated using a water-budget model for the island of Maui, Hawai'i, 1978–2007. U.S. Geological Survey Scientific Investigations Report 2014–5168.
- Kaushal, S.S., Grossman, P.M., Band, L.E., Elliott, E.M., Shields, C.A., Kendall, C., 2011. Tracking nonpoint source nitrogen pollution in human-impacted watersheds. *Environ. Sci. Technol.* 45, 8225–8232, <http://dx.doi.org/10.1021/es200779e>, <http://pubs.acs.org/jpdf/10.1021/es200779e>.
- Keith, T.Z., 2006. *Multiple Regression and Beyond*, 2nd ed. Pearson Education, Boston, MA, 534 p.
- Kelly, J.K., (2012). Identification and quantification of submarine groundwater discharge in the Hawaiian Islands. Ph.D. Dissertation from the Department of Geology and Geophysics, 81 p, Honolulu Hawai'i: University of Hawai'i at Manoa.
- Kelly, J.L., Glenn, C.R., 2015. Chlorofluorocarbon apparent ages of groundwaters from west Hawai'i USA. *J. Hydrol.*, <http://dx.doi.org/10.1016/j.jhydrol.2015.04.069>.
- Kendall, C., 1998. Tracing nitrogen sources and cycling in catchments. In: Kendall, C., McDonnell, J.J. (Eds.), *Isotope Tracers in Catchment Hydrology*. Elsevier, Amsterdam, pp. 519–576, <http://www.wrcoml.wr.usgs.gov/isoig/ispubs/itchch16html>.
- Knee, K.L., Layton, B., Street, J.H., Boehm, A., Paytan, A., 2008. Sources of nutrients and fecal indicator bacteria to nearshore waters on the north shore of Kauai (Hawai'i, USA). *Estuar. Coasts*, <http://dx.doi.org/10.1007/s12237-008-9055-6>.
- Knee, K.L., Street, J.H., Grossman, E.E., Boehm, A.B., Paytan, A., 2010. Nutrient inputs to the coastal ocean from submarine groundwater discharge in a groundwater-dominated system: Relation to land use (Kona coast, Hawai'i, U.S.A.). *Limnol. Oceanogr.* 55, 1105–1122, <http://dx.doi.org/10.4319/lo.2010.55.3.1105>.
- Lapworth, D.J., Goody, D.C., Kent, F., Heaton, T.H.E., Cole, S.J., Allen, D., 2013. A combined geochemical and hydrological approach for understanding macronutrient sources. *J. Hydrol.* 500, 226–242, <http://dx.doi.org/10.1016/j.jhydrol.2013.07.006>.
- Laws, E., Brown, D., Peace, C., 2004. Coastal water quality in the Kihei and Lahaina districts of the island of Maui, Hawaiian Islands. *Impacts from physical habitat and groundwater seepage: Implications for water quality standards*. *Int. J. Environ. Pollut.* 22, 531–546.
- Mann, K.H., 2000. *Ecology of Coastal Waters with Implications for Management*, 2nd ed. Wiley Blackwell, 432 p.
- McIlvin, M.R., Casciotti, K.L., 2011. Technical updates to the bacterial method for nitrate isotopic analyses. *Anal. Chem.* 54, 1850–1856, <http://dx.doi.org/10.1021/ac1028984>.
- McMahon, P.B., Bohlke, J.K., 2006. Regional patterns in the isotopic composition of natural and anthropogenic nitrate in groundwater, High Plains, U.S.A. *Environ. Sci. Technol.* 40, 2965–2970, <http://dx.doi.org/10.1021/es052229q>.
- Nelson, J.L., Zavaleta, E.S., 2012. Salt marshes as a coastal filter for oceans: Changes in function with experimental increases in nitrogen loading and sea-level rise. *PLoS One* 7, e38558, <http://dx.doi.org/10.1371/journal.pone.0038558>.
- NOAA, (2012). National Oceanic and Atmospheric Administration (NOAA). Coastal Change Analysis Program Regional Land Cover (C-CAP) Hawai'i 2005 Land Cover. NOAA Ocean Service, Office for Coastal Management. <http://coast.noaa.gov/digitalcoast/data/ccapregional>.
- NOAA, (2007). National Oceanic and Atmospheric Administration (NOAA). Digital elevation models for the main 8 Hawaiian islands. National Ocean Service, National Center's for Coastal ocean Science, Silver Springs, MD. <http://ccma.nos.noaa.gov/products/biogeography/mapping/dems/>.
- Paytan, A., Shellenberger, G.G., Street, J.H., Gonnee, M., Davis, K., Young, M.B., Moore, W.S., 2006. Submarine groundwater discharge: An important source of new inorganic nitrogen to coral reef ecosystems. *Limnol. Oceanogr.* 51, 343–348, <http://dx.doi.org/10.4319/lo.2006.51.1.0343>.
- Pollock, D.W., (2012). User guide for MODPATH version 6–A particle-tracking model for MODFLOW U.S. Geological Survey Techniques and Methods 6–A41, 58 p. <http://pubs.usgs.gov/tm/6a41/>.
- Robertson, W.D., Cherry, J.A., Sudicky, E.A., 1991. Ground-water contamination from two small septic systems on sand aquifers. *Groundwater* 29, 82–92.
- Robertson, W.D., Schiff, S.L., Ptacek, C.J., 1998. Review of phosphate mobility and persistence in 10 septic system plumes. *Groundwater* 36, 1000–1010.
- Santos, I.R., Burnett, W.C., Chanton, J., Mwashote, B., Suryaputra, I.G.N.A., Dittma, T., 2008. Nutrient biogeochemistry in a Gulf of Mexico subterranean estuary and groundwater derived fluxes to the coastal ocean. *Limnol. Oceanogr.* 53, 705–718.
- Scholl, M.A., Gingerich, S.B., Tribble, C.W., 2002. The influence of microclimates and fog on stable isotope signatures used in interpretation of regional hydrology, East Maui, Hawai'i. *J. Hydrol.* 170–184, 2–00073, [http://dx.doi.org/10.1016/S0022-1694\(02\)](http://dx.doi.org/10.1016/S0022-1694(02)).
- Scholl, M.A., Ingebritsen, S.E., Janik, C.J., Kaauhikaua, J.P., 1996. Use of precipitation and groundwater isotopes to interpret regional hydrology on a tropical volcanic island: Kilauea volcano area, Hawai'i. *Water Resour. Res.* 32, 3525–3537, <http://dx.doi.org/10.1029/95wr02837>.
- Singleton, M.J., Woods, K.N., Conrad, M.E., DePaolo, D.J., Dresel, P.E., 2005. Tracking sources of unsaturated zone and groundwater nitrate contamination using nitrogen and oxygen stable isotopes at the Hanford Site, Washington. *Environ. Sci. Technol.* 39, 3563–3570, <http://dx.doi.org/10.1021/es0481070>.
- Sigman, D.M., Casciotti, K.L., Andreani, M., Barford, C., Galanter, M., Bohlke, J.K., 2001. A bacterial method for the nitrogen isotopic analysis of nitrate in seawater and freshwater. *Anal. Chem.* 73, 4145–4153, <http://dx.doi.org/10.1021/ac010088e>.
- Soicher, A.J., Peterson, F.L., 1997. Terrestrial nutrient and sediment fluxes to the coastal waters of West Maui, Hawai'i. *Pac. Sci.* 51 (1997), 221–232, <http://scholarspace.manoa.hawaii.edu/bitstream/handle/10125/3143/v51n3-221-232pdf?sequence=1>.
- State of Hawai'i (2008). Water Resource Protection Plan, June 2008: Commission on Water Resource Management, 556 p.
- Stearns, H.T., Macdonald, G.A., 1942. *Geology and groundwater resources of the island of Maui, Hawai'i*. U.S. Geol. Survey Bull., 7.
- Street, J.H., Knee, K.L., Grossman, E.E., Paytan, A., 2008. Submarine groundwater discharge and nutrient addition to the coastal zone and coral reefs of leeward Hawai'i. *Mar. Chem.* 109, 355–376, <http://dx.doi.org/10.1016/j.marchem.2007.08.009>.
- Swarzenski, P.W., Storlazzi, C.D., Presto, M.K., Gibbs, A.E., Smith, C.G., Dimova, N.T., Dailer, M.L., Logan, J.B., (2012). Nearshore morphology, benthic structure, hydrodynamics, and coastal groundwater discharge near Kahekili Beach Park, Maui, Hawai'i. U.S. Geological Survey Open File Report 2012–1166. <http://pubs.usgs.gov/of/2012/1166/>.
- Swarzenski, P.W., Dulaiova, H., Dailer, M.L., Glenn, C.R., Smith, C.G., Storlazzi, C.D., 2013. A geochemical and geophysical assessment of coastal groundwater discharge at select sites in Maui and O'ahu, Hawai'i. In: *Groundwater in the Coastal Zones of Asia-Pacific*. Springer, Netherlands, pp. 27–46.
- Tetra Tech, Inc., (1994). Effluent fate study, Lahaina wastewater reclamation facility, Maui, Hawai'i: Prepared for U.S. Environmental Protection Agency Region 9, 73p. plus appendices.
- van Beukering, P.J.H., Cesar, H.S.J., 2004. Ecological economic modeling of coral reefs: Evaluating tourist overuse at Hanauma Bay and algae blooms at the Kihei coast, Hawai'i. *Pac. Sci.*, v. 58, 243–260, <http://dx.doi.org/10.1353/psc.2004.0012>.
- Visher, F.N., Mink, J.F., (1964). Groundwater resources in Southern Oahu, Hawai'i. USGS Open File Report 1778.
- Vitousek, P., 2004. *Nutrient Cycling and Limitation: Hawai'i as a Model System*. Princeton University Press, Princeton New Jersey, 232 p.
- Wankel, S.D., Kendall, K., Francis, C.A., Paytan, A., 2006. Nitrogen sources and cycling in the San Francisco Bay Estuary: a nitrate dual isotopic composition approach. *Limnol. Oceanogr.* 51, 1654–1664, <http://dx.doi.org/10.4319/lo.2006.51.4.1654>.
- Weigner, T.N., Tubal, R.L., MacKenzie, R.A., 2009. Bioavailability and export of dissolved organic matter from a tropical river during base and stormflow conditions. *Limnol. Oceanogr.*, 1233–1242, <http://dx.doi.org/10.4319/lo.2009.54.4.1233>, http://www.aslo.org/lo/toc/vol_54/issue_4/1233.pdf.
- Whittier, R.B., Rotzoll, K., Dhal, S., El-Kadi, A.I., Ray, C., Chang, D., 2010. Groundwater source assessment program for the state of Hawai'i, USA: methodology and example application. *Hydrogeol. J.* 18, 711–723, <http://dx.doi.org/10.1007/s10040-009-0548-6>, <http://link.springer.com/article/10.1007/s10040-009-0548-6>.
- Whittier, R. B., El-Kadi, A. I., (2014). Human health and environmental risk ranking of onsite sewage disposal systems for the Hawaiian Islands of Kauai, Maui, Molokai, and Hawai'i. Report submitted, State of Hawai'i Department of Health and Safe Drinking Water Branch, Honolulu, HI, 258 pp.
- Yates, M.V., 1985. Septic tank density and groundwater contamination. *Groundwater* 23, 586–591, <http://dx.doi.org/10.1111/j.1745-6584.1985.tb01506.x>.
- Young, C., Tamborski, J., Bokuniewicz, H., (2015). Embayment scale assessment of submarine groundwater discharge nutrient loading an associated land use. *Est., Coast., and Shelf Sci.*, 158 (2015), p.20–30. 10.1016/j.ecss.2015.02.006 <http://www.sciencedirect.com/science/article/pii/S0272771415000530#>.